11-1-2001

Variational Transition State Theory Evaluation Of The Rate Constant For Proton Transfer In A Polar Solvent

Robin P. McRae
Eastern Washington University, rmcrae@ewu.edu

Gregory K. Schenter

Bruce C. Garrett

Zoran Svetlicic

Donald G. Truhlar

Variational transition state theory evaluation of the rate constant for proton transfer in a polar solvent

Robin P. McRae
Department of Chemistry, Eastern Washington University, Cheney, Washington 99004

Gregory K. Schenter and Bruce C. Garrett
Environmental Molecular Sciences Laboratory, Pacific Northwest National Laboratory, Richland, Washington 99352

Zoran Svetlicic and Donald G. Truhlar
Department of Chemistry and Supercomputer Institute, University of Minnesota, Minneapolis, Minnesota 55455

(Received 16 May 2001; accepted 17 August 2001)

Variational transition state theory (VTST) is used to calculate rate constants for a model proton transfer reaction in a polar solvent. We start from an explicit description of the reacting solute in a solvent, and we model the effects of solvation on the reaction dynamics by a generalized Langevin equation (GLE) for the solute. In this description, the effects of solvation on the reaction energetics are included in the potential of mean force, and dynamical, or nonequilibrium, solvation is included by solvent friction. The GLE solvation dynamics are approximated by a collection of harmonic oscillators that are linearly coupled to the coordinates of the reacting system. This approach is applied to a model developed by Azzouz and Borgis [J. Chem. Phys. **98**, 7361 (1993)] to represent proton transfer in a phenol-amine complex in liquid methyl chloride. In particular, semiclassical VTST, including multidimensional tunneling contributions, is applied to this model with three explicit solute coordinates and a multioscillator GLE description of solvation to calculate rate constants. We compare our computed rate constants and H/D kinetic isotope effects to previous calculations using other approximate dynamical theories, including approaches based on one-dimensional models, molecular dynamics with quantum transitions, and path integrals. By examining a systematic sequence of 18 different sets of approximations, we clarify some of the factors (such as classical vibrations, harmonic approximations, quantum character of reaction-coordinate motion, and nonequilibrium solvation) that contribute to the different predictions of various approximation schemes in the literature. © *2001 American Institute of Physics.* [DOI: 10.1063/1.1409953]

I. INTRODUCTION

Proton transfer reactions are encountered frequently in chemistry and biochemistry.[1,2] Proton transfer reactions in solution are central to acid and base catalysis in aquatic environments[3] and to enzyme-catalyzed reactions.[2] The theoretical treatment of proton transfer in solution is especially difficult for two reasons. First, polar solvent environments (e.g., aqueous solutions) profoundly affect charge transfer processes, such as proton transfer, and the explicit treatment of the important solvent effects, such as orientational polarization, require consideration of collective motions and large molecular ensembles in computer simulations. Second, proton motion involves quantum mechanical behavior such as zero-point energy constraints and tunneling, requiring a quantum mechanical treatment that is a computational challenge in many-body systems. Although we explicitly discuss proton transfer in the present article, similar considerations apply to hydride transfer.

A variety of theoretical methods have been developed and applied to proton transfer reactions.[4–15] Transition state theory (TST)[16–19] is one of the most prevalent theoretical approaches to reaction rates in general and proton transfer in particular, and many of the approaches cited above incorporate elements of TST. A particularly successful TST approach is based on variational transition state theory with multidimensional tunneling (VTST/MT)[19,20] in which vibrational partition functions are quantized and quantum mechanical effects on reaction coordinate motion are included by semiclassical multidimensional tunneling approximations. This approach has been very successful at predicting gas-phase reaction rate constants,[21,22] has been extended to reactions in solution,[10,23–27] and has been extended to proton and hydride transfer reactions in enzymes.[15,28] Although limited tests of the VTST/MT approach to reactions in solution have been presented, these applications have all employed a model for the reaction in solution based upon a generalized Langevin equation (GLE)[29–31] approach. In the current work we wish to test the VTST/MT approach by starting from an explicit molecular model for the reaction system.

Azzouz and Borgis[7] presented a model for the proton transfer reaction

$$\mathrm{AH}-\mathrm{B}\leftrightarrow\mathrm{A}^{-}-\mathrm{H}^{+}\mathrm{B} \tag{1}$$

in a polar solvent. The chemical groups AH and B represent

a weak acid such as phenol and a weak base such as an amine, respectively, and the polar solvent is a model for methyl chloride. Azzouz and Borgis[7,8,11] calculated rate constants for this model using a semiclassical curve-crossing approach[6] and a path integral quantum TST approach.[5,32] Subsequently Hammes-Schiffer and Tully[9] used a surface hopping approach (molecular dynamics with quantum transitions)[33] to calculate rate constants. In the surface hopping approach the continuous motion of the classical subsystem on an effective potential surface generated by the quantum subsystem is interrupted by discontinuous hops corresponding to quantum transitions. More recently, Antoniou and Schwartz[12–14] performed calculations of rate constants using an evolution operator technique[34] based upon the flux correlation function formalism,[35] which is another method that is closely related to TST.[19,36] Azzouz and Borgis also presented a ''corrected'' classical TST approach in which one-dimensional TST rate constants, including quantization of the proton motion and tunneling based on a parabolic barrier approximation,[37,38] were averaged over fixed A–B separations. In the work of Azzouz and Borgis and Hammes-Schiffer and Tully the proton motion was treated quantum mechanically, while the other coordinates in the system were treated classically. The approach taken by Antoniou and Schwartz treated the solvent using a GLE, in which the effects of solvent dynamics were included by a harmonic bath coupled linearly to the reaction coordinate,[39] i.e., to the proton motion between A and B; the one-dimensional solute and the harmonic bath coordinates were treated quantum mechanically in their approach. In the present work we also reduce the solvent dynamics to a GLE, but the solute is treated multidimensionally including the proton motion, heavy-atom A–B motion, and center-of-mass AHB motion. In the present article we treat the dynamics of all degrees of freedom of the reduced model on an equal footing by using semiclassical VTST/MT, and we also present a systematic series of more approximate calculations.

The organization of the remainder of this paper is as follows. Section II describes the model of Azzouz and Borgis, and Sec. III presents the VTST/MT approach that we use for this model, including the development of the GLE and application of VTST. Section IV provides computational details, Sec. V presents results and discussion, and Sec. VI gives conclusions from this study.

II. MODEL SYSTEM

The specific system studied here is a model of a triatomic reactive complex dissolved in a polar solvent. The parameters of the system are chosen so that the reactive complex represents a proton transfer reaction from a phenol to a trimethylamine, and the solvent molecules are representative of methyl chloride. This model is chosen to be essentially identical to that used by Azzouz and Borgis,[7] Hammes-Schiffer and Tully,[9] and Antoniou and Schwartz[13,14] in their respective works.

The model constrains the proton transfer reaction to take place in one dimension; bending modes are completely disallowed. Further, the ''phenolate'' (A^-) and ''trimethylamine'' (B) groups are represented in a united atom sense, so that the reaction model is a three-atom collinear system as shown in Eq. (1). The masses of A and B, m_A and m_B, are set to 93 and 59 amu, respectively, while the mass of H, m_H, is set to 1 amu for proton transfer or 2 amu for deuteron transfer. An important aspect of this model is that the distribution of charges within the complex depends on the location of the proton, much as one would expect. As the proton shifts from the phenol side to the amine side within the complex, the reactive complex changes from a polar but neutral complex into an ion pair. This in turn causes a large change in dipole moment in the course of the reaction and allows for a strong interaction between the complex and the surrounding polar solvent.

The geometry of the AHB complex is described by the Cartesian vectors for atoms A, H, and B, denoted by $\mathbf{r}_A$, $\mathbf{r}_H$, and $\mathbf{r}_B$, respectively, or by the position of its center-of-mass, $\mathbf{R}_{CM}$, a unit orientation vector $\hat{\mathbf{z}}$ pointing from atom A toward atom B, and the scalar distances $r=|\mathbf{r}_A-\mathbf{r}_H|$ and $R=|\mathbf{r}_A-\mathbf{r}_B|$. The orientation vector is characterized by the polar coordinates $(\theta,\ \phi)$, as $\hat{\mathbf{z}}=(\sin\theta\cos\phi, \sin\theta\sin\phi,\cos\theta)$. Since the proton is constrained to lie along the A–B bond, its coordinate can be described by the single variable r such that

$$\mathbf{r}_H=\mathbf{r}_A+\hat{\mathbf{z}}r. \tag{2}$$

The potential energy of the complex is denoted $V_{HB}(r,R)$. In this case the Hamiltonian for the complex, in the absence of the solvent, is described in terms of seven coordinates and their conjugate momenta

$$H_{gas}=\frac{\mathbf{P}_{CM}^2}{2M}+\frac{1}{2I}\left(P_\theta^2+\frac{P_\phi^2}{\sin^2\theta}\right)+\frac{1}{2}(P_r,P_R)\boldsymbol{\mu}^{-1}\begin{pmatrix}P_r\\P_R\end{pmatrix}+V_{HB}(r,R), \tag{3}$$

where the kinetic energy is expressed in terms of the momentum conjugate to θ and ϕ, P_θ and P_ϕ, the momentum of the center-of-mass of the complex $\mathbf{P}_{CM}$, and the momenta P_r and P_R, which are conjugate to r and R. The effective mass matrix, $\boldsymbol{\mu}$, is explicitly given by

$$\boldsymbol{\mu}=\frac{1}{M}\begin{pmatrix}(m_A+m_B)m_H & -m_Hm_B\\ -m_Hm_B & (m_A+m_H)m_B\end{pmatrix}, \tag{4}$$

where $M=m_A+m_H+m_B$ is the total mass of the complex. The scalar moment of inertia along the collinear axis is:

$$I(r,R)=(r,R)\boldsymbol{\mu}\begin{pmatrix}r\\R\end{pmatrix}. \tag{5}$$

In the limit that $m_H\ll m_A$ and $m_H\ll m_B$,

$$\boldsymbol{\mu}\approx\begin{pmatrix}m_H & 0\\ 0 & \mu_{AB}\end{pmatrix}, \tag{6}$$

where $\mu_{AB}=m_Am_B/(m_A+m_B)$, and the moment of inertia in Eq. (5) is approximated by $\mu_{AB}R^2$. As noted previously,[7] with this approximation the proton motion is no longer di-

TABLE I. Parameters for the gas-phase potential.

Parameter	Value
a	11.2 Å^{-1}
b	7.1×10^{13} kcal/mol
d_A	0.95 Å
d_B	0.97 Å
D_A	110 kcal/mol
n_A	9.26 Å^{-1}
n_B	11.42 Å^{-1}
c	0.776

rectly coupled to the overall rotation of the complex. In the approach described below it is not necessary to make this approximation, and so we retain the coupled expression of Eq. (4) in the molecular simulations, although we do use $I \cong \mu_{AB}R^2$ to construct the potential of mean force, and this approximation is excellent for the system studied here.

The gas-phase potential energy function is given by

$$V_{HB}(r,R) = b\exp(-aR) + D_A\left\{1-\exp\left[\frac{-n_A(r-d_A)^2}{2r}\right]\right\} + cD_A\left\{1-\exp\left[\frac{-n_B(R-r-d_B)^2}{2(R-r)}\right]\right\}. \quad (7)$$

The values of the parameters used in this study are taken directly from Hammes-Schiffer and Tully[9] and are given in Table I for convenience. Note that these parameters are also very similar to those used for "Model II" by Azzouz and Borgis.[7]

The methyl chloride solvent is represented with the model used by Bigot *et al.*[40] in their Monte Carlo simulations. This is not only the same solvent model as was used in the aforementioned proton transfer studies; it has also been used to examine properties of pure methyl chloride. The Bigot model treats the methyl chloride molecule as a rigid, polar, diatomic nonpolarizable molecule, with the methyl group being treated as a united atom at a distance of 1.78 Å from the chlorine atom. The mass of the methyl united atom m_{Me} is 15 amu and that of the chlorine atom m_{Cl} is 35 amu. The Cartesian vectors for the methyl and chlorine in solvent molecule k are denoted $\mathbf{r}_k^{Me}$ and $\mathbf{r}_k^{Cl}$ with conjugate momentum $\mathbf{p}_k^{Me}$ and $\mathbf{p}_k^{Cl}$. The Hamiltonian for the entire model system (complex plus solvent) is written as a sum of three distinct parts:

$$H = H_{gas} + H_{solvent} + V_{CS}(r,R,\mathbf{R}_{CM},\hat{\mathbf{z}},\mathbf{R}_S) \quad (8)$$

which yields

$$H = H_{gas} + \sum_k \sum_{\beta=Me,Cl} \frac{(\mathbf{p}_k^\beta)^2}{2m_\beta} + V_{SS}(\mathbf{R}_S) + V_{CS}(r,R,\mathbf{R}_{CM},\hat{\mathbf{z}},\mathbf{R}_S), \quad (9)$$

where $\mathbf{R}_S$ is the collection of all solvent coordinates, $V_{SS}(\mathbf{R}_S)$ is the solvent–solvent potential, and $V_{CS}(r,R,\hat{\mathbf{z}},\mathbf{R}_{CM},\mathbf{R}_S)$ is the potential that couples the complex to the solvent molecules.

TABLE II. Parameters for the methyl chloride solvent model.

Atom	$q(e)$	A^2 (kcal mol^{-1} Å^{12})	C^2 (kcal mol^{-1} Å^6)
CH_3	+0.25	7.95×10^6	2750
Cl	−0.25	5.25×10^6	2950

Interactions between solvent molecules include both Lennard-Jones and Coulomb potentials between each of the atomic sites on the interacting molecules. The solvent–solvent potential energy is given by the TIPS (Transferable Intermolecular Potential Functions) model,[41] following the description given by Hammes-Schiffer and Tully[9]

$$V_{SS}(\mathbf{R}_S) = \frac{1}{2}\sum_{k\neq k'}\sum_{\beta,\beta'=Me,Cl}\left(\frac{q_\beta q_{\beta'}}{|\mathbf{r}_k^\beta - \mathbf{r}_{k'}^{\beta'}|} + \frac{A_\beta A_{\beta'}}{|\mathbf{r}_k^\beta - \mathbf{r}_{k'}^{\beta'}|^{12}} - \frac{C_\beta C_{\beta'}}{|\mathbf{r}_k^\beta - \mathbf{r}_{k'}^{\beta'}|^6}\right). \quad (10)$$

Parameters q_β, A_β, and C_β for β=Me and Cl are given in Table II. With the charges indicated in this table, the dipole moment of a solvent molecule is 2.14 D.

The interaction potential energy between the solvent and the dissolved reactive complex consists of Coulomb potentials between solvent molecules and atoms A, B, and H and Lennard-Jones potentials between solvent molecules and atoms A and B (but not the H atom)

$$V_{CS}(r,R,\mathbf{R}_{CM},\hat{\mathbf{z}},\mathbf{R}_S) = \sum_{\alpha=A,B,H}\sum_k\sum_{\beta=Me,Cl}\frac{q_\alpha(r)q_\beta}{|\mathbf{r}_\alpha - \mathbf{r}_k^\beta|} + \sum_{\alpha=A,B}\sum_k\sum_{\beta=Me,Cl} \times 4\epsilon\left[\left(\frac{\sigma}{|\mathbf{r}_\alpha - \mathbf{r}_k^\beta|}\right)^{12} - \left(\frac{\sigma}{|\mathbf{r}_\alpha - \mathbf{r}_k^\beta|}\right)^6\right], \quad (11)$$

where $\mathbf{r}_\alpha$ is an implicit function of r, R, $\mathbf{R}_{CM}$, and $\hat{\mathbf{z}}$. The charges on the atoms in the complex range from their values in the "covalent" state, $q_A^c = -0.5e$, $q_H^c = +0.5e$, $q_B^c = 0$, to their values in the "ionic" state, $q_A^i = -1.0e, q_H^i = +0.5e, q_B^i = +0.5e$ by means of a smooth, r-dependent switching function:

$$q_\alpha(r) = [1-f(r)]q_\alpha^c + f(r)q_\alpha^i, \quad (12)$$

where

$$f(r) = \frac{1}{2}\left(\frac{r-l}{\sqrt{(r-l)^2+(\Delta l)^2}}\right), \quad (13)$$

with $l = 1.43$ Å and $\Delta l = 0.125$ Å. This charge switching causes the dipole moment of the reactive solute complex to vary from 2.5 D in the covalent state to 10.5 D in the ionic state. The Lennard-Jones potentials between atoms A or B and either of the sites on a methyl chloride molecule are identical: $\sigma = 3.5$ Å and $\epsilon = 200$ K. The Coulomb part of the interaction involves the usual potential between the fixed

point charges on the atomic sites of the solvent molecules and the *r*-dependent point charges located on each of the three atoms in the complex.

III. VARIATIONAL TRANSITION STATE APPROACH FOR REACTIONS IN LIQUID SOLUTION

The approach we use here to calculate the rate of proton transfer in this model reaction in liquid solution is based on variational transition state theory. The general approach has been described previously,[25] and the details of the implementation have been presented elsewhere.[23,24,26,27] Our approach to VTST in the gas phase[19,20] requires locating critical geometries (minima and saddle points) and minimum energy pathways on the global potential energy surface. However, we need to extend this approach for reactions in liquids, like the present model system, since the full-dimensional potential energy surface of such reactions will exhibit many local minima and saddle points corresponding to many possible equilibrium geometries of the solvent molecules, with little rearrangement of the atoms in the reactive complex. In this work we take an approach described earlier,[23–27] in which we center attention not on the full-system potential energy surface but rather on the solute potential of mean force and the friction tensor due to the solvent. Thus the dynamics of the reactive complex and the equilibrium solvent effects are treated by a potential of mean force surface, and nonequilibrium solvent effects are treated by solvent friction terms that are approximated by a generalized Langevin equation.

We first discuss the development of the generalized Langevin equation for this model system, including the calculation of the multidimensional potential of mean force surface and friction tensor. The procedure we use to map the GLE onto Hamiltonian dynamics, employing a GLE Hamiltonian, is then described. Finally we review how VTST/MT is applied to the GLE Hamiltonian.

III.A. Generalized Langevin equation

As has been discussed in many of the references given in the introduction, there are a number of ways in which a solvent can interact with a dissolved reactive system to alter the reaction rate relative to that for the same reaction in the gas phase. The influences of the solvent can be classified into three categories: (i) explicit solvent participation in the reaction, such as bond making or bond breaking in solvent molecules (as in general acid-base catalysis), or some types of explicit solute ''caging'' interactions; (ii) equilibrium solvation effects on the potential of mean force experienced by the reactive system; and (iii) nonequilibrium solvation effects, i.e., the frictional effect of the solvent on the reactive system. Effects of types (i) and (iii) involve solvent participation in the reaction coordinate, whereas effects of type (ii) do not. Effects of types (ii) and (iii) can be treated by either implicit[42] or explicit[43] solvation models, whereas effects of type (i) always require explicit solvent. The treatment employed in the present article does not consider any type (i) effects, although, if important, such effects could be incorporated within the general framework of this method by including solvent molecules explicitly in the ''solute'' reactive system—that is, redefining the reactive system to include certain solvent molecules. The dynamical scheme used here treats solvent implicitly via collective solvent coordinates. The method is general enough that input data for the implicit-solvent dynamical treatment could be obtained from either implicit solvation models or explicit solvation models.[24,26,44] As we will see in Sec. IV, we shall use the latter approach in the present article. First, however, in this section and Secs. III B and III C, we shall establish the dynamical model for reaction (1).

We begin by concentrating on a reduced set of coordinates and modeling the solvent effects using a generalized Langevin equation. The occurrence of a reactive event in this system is determined by motion of the proton from species A to B and for the most part this is determined by progress in the *r* coordinate. Thus, as in other studies of this model system,[7,9,13,14] we treat the proton motion explicitly. In previous studies,[23,26,27] we found that coupling between the heavy-atom motion (A–B relative motion) and light-atom transfer can have significant effects on the reaction. In addition, coupling between the center-of-mass translation and proton transfer can also be significant when solvent friction has a high value.[27] Therefore in the current study we wish to retain an explicit treatment of *r, R,* and the center-of-mass motion along the A–B axis. To accomplish this we define a reduced system consisting of the three coordinates describing the motion of the three atoms that are constrained to be along the line connecting A and B. In particular, we define the three coordinates, (z_A, z_H, z_B), where

$$\mathbf{r}_\alpha = \mathbf{R}_{CM} + \hat{\mathbf{z}} z_\alpha, \quad \alpha = \mathrm{A,B,H}. \tag{14}$$

The same transformation matrix,

$$\mathbf{A} = \begin{pmatrix} -1 & 0 & 1 \\ -1 & 1 & 0 \\ \dfrac{m_A}{M} & \dfrac{m_B}{M} & \dfrac{m_H}{M} \end{pmatrix} \tag{15}$$

that connects the coordinates defined in Sec. II, i.e.,

$$\begin{pmatrix} \mathbf{r} \\ \mathbf{R} \\ \mathbf{R}_{CM} \end{pmatrix} = \mathbf{A} \begin{pmatrix} \mathbf{r}_A \\ \mathbf{r}_B \\ \mathbf{r}_H \end{pmatrix}, \tag{16}$$

may be used to define the reduced, transformed coordinates

$$\begin{pmatrix} r \\ R \\ Z_{CM} \end{pmatrix} = \mathbf{A} \begin{pmatrix} z_A \\ z_B \\ z_H \end{pmatrix}. \tag{17}$$

Note that a consequence of the transformation, Eq. (17), is that Z_{CM} always equals 0.

Similarly to the work of Azzouz and Borgis,[7] we define a collective set of bath coordinates **S** that includes the orientational coordinates and the center-of-mass coordinates of the solute as well as the collection $\mathbf{R}_S$ of solvent coordinates, $\mathbf{S} = (\theta, \phi, \mathbf{R}_{CM}, \mathbf{R}_S)$. With this definition of the solvent, we could construct a GLE in terms of the (r,R) coordinates alone, or equivalently, in terms of (z_A, z_B, z_H) where the constraint $Z_{CM} = 0$ is imposed. This GLE does not account for dynamical coupling between the *r* and *R* coordinates due to the solute center-of-mass translational motion in the solvent,

which was found to be important in a previous study.[27] A simple way to introduce this dynamical coupling is to relax the constraint that Z_{CM} is equal to 0 and allow dynamical motion in Z_{CM}. The equations of motion for the three explicit coordinates in the GLE approach are then written[30]

$$m_\alpha \ddot{z}_\alpha = -\frac{\partial}{\partial z_\alpha} W + \int_0^t dt' \sum_{\alpha'} \eta_{\alpha\alpha'}(t-t')\dot{z}_{\alpha'}(t') + \delta F_\alpha(t), \quad \alpha = \mathrm{A,B,H}, \tag{18}$$

where the components of the mean force are defined by

$$\frac{\partial W}{\partial z_\alpha} = \left\langle \frac{\partial H}{\partial z_\alpha} \right\rangle_{r,R}, \tag{19}$$

where W is the potential of mean force, H is the Hamiltonian defined by Eqs. (3) and (8), and the averages $\langle \cdots \rangle_{r,R}$ are over bath coordinates **S** with the internal coordinates of the solute fixed. The friction tensor $\eta_{\alpha\alpha'}$ is defined by

$$k_{\mathrm{B}} T \eta_{\alpha\alpha'}(t) = \langle \delta F_\alpha(t)\, \delta F_{\alpha'}(0) \rangle_{r,R}, \tag{20}$$

where k_{B} is Boltzmann's constant, T is the temperature of the system, F_α is the α component of the force in the **z** coordinate system, and the fluctuation in the force on solute coordinate α due to the instantaneous bath configuration is given by

$$\begin{aligned} \delta F_\alpha(t) &\equiv F_\alpha(t) - \langle F_\alpha \rangle_{r,R} \\ &= -\frac{\partial H}{\partial z_\alpha}(t) + \left\langle \frac{\partial H}{\partial z_\alpha} \right\rangle_{r,R} \\ &= -\frac{\partial H}{\partial z_\alpha}(t) + \frac{\partial W}{\partial z_\alpha}. \end{aligned} \tag{21}$$

In taking the averages in Eqs. (19) and (21), we choose the values of r and R that correspond to the saddle point of W.

Note that the constraints on the averages in Eqs. (19)–(21) involve the coordinates r and R, whereas the GLE is for the three coordinates including Z_{CM} as well as (r,R). Although the constraints should also include Z_{CM}, the effect on the GLE from not including it is negligible, as explained below. First, consider the mean force defined in Eq. (19). In the gas phase, the internal motion of the solute is decoupled from the center-of-mass translation, so $\partial V_{\mathrm{HB}}/\partial Z_{\mathrm{CM}}$, is zero. Although $\partial V_{\mathrm{CS}}/\partial Z_{\mathrm{CM}}$ is in general nonzero because of unsymmetrical contributions of solvent molecules, the average of $\partial V_{\mathrm{CS}}/\partial Z_{\mathrm{CM}}$ over solvent configurations is zero. Therefore, since $\partial W/\partial Z_{\mathrm{CM}} = 0$, W does not change if Z_{CM} is constrained. Next, consider the friction tensor appearing in the GLE and defined by Eqs. (20) and (21). The force fluctuations defined in Eq. (21) depend on instantaneous values of $\partial V_{\mathrm{CS}}/\partial Z_{\mathrm{CM}}$, which are not necessarily zero, and may exhibit correlations with values at other times. Therefore the friction tensor will have an explicit dependence on Z_{CM}. We have tested the sensitivity of the friction tensor to constraints with numerical simulation. The friction tensor was computed with just r and R constrained and compared with the friction tensor compute with r, R, and $\mathbf{R}_{\mathrm{CM}}$ constrained. No numerically significant differences were observed for the friction tensors computed with the two different constraints. Our assumption is that the friction tensor with r, R, and Z_{CM} constrained would also show no significant differences.

For the present study we approximate the dynamics of the GLE in Eq. (18) by the dynamics determined by an effective Hamiltonian given by[39,45]

$$H_{\mathrm{GLE}} = \sum_{\alpha=\mathrm{A,B,H}} \frac{P_{z\alpha}^2}{2m_\alpha} + W(r,R) + \sum_{j=1}^{N} \left\{ \frac{P_{yj}^2}{2m_b} + \frac{1}{2} m_b \omega_j^2 \left(y_j - \sum_{\alpha=\mathrm{A,B,H}} C_{j\alpha} z_\alpha \right)^2 \right\}, \tag{22}$$

where N is the number of effective solvent degrees of freedom, $P_{z\alpha}$ is the momentum conjugate to z_α, and y_j and P_{yj} are effective dynamical solvent coordinates and momentum providing nonequilibrium solvent effects on the dynamical motion. The value of the effective solvent mass m_b is arbitrary, while the solvent frequencies ω_j and coupling constants $C_{j\alpha}$ characterize the effective solvent response to the reduced coordinate motion. The classical dynamics of this effective Hamiltonian approximates the dynamics generated by Eq. (18), when the friction tensor is given in terms of the bath parameters ω_j and $C_{j\alpha}$ by[39,45]

$$\eta_{\alpha\alpha'}(t) = \sum_{j=1}^{N} m_b C_{j\alpha} C_{j\alpha'} \omega_j^2 \cos(\omega_j t). \tag{23}$$

The effective GLE Hamiltonian may also be written in terms of the (r,R,Z_{CM}) coordinates as

$$H_{\mathrm{GLE}} = \frac{P_{Z_{\mathrm{CM}}}^2}{2M} + \frac{1}{2}(P_r, P_R)\boldsymbol{\mu}^{-1}\begin{pmatrix} P_r \\ P_R \end{pmatrix} + W(r,R) + \sum_{j=1}^{N} \left\{ \frac{P_{yj}^2}{2m_b} + \frac{1}{2} m_b \omega_f^2 (y_j - \tilde{C}_{j,r} r - \tilde{C}_{j,R} R - \tilde{C}_{j,\mathrm{CM}} Z_{\mathrm{CM}})^2 \right\}, \tag{24}$$

where

$$\tilde{\mathbf{C}} = \mathbf{C}\mathbf{A}^{-1}. \tag{25}$$

Specific details of the simulation procedure used for the construction of the GLE Hamiltonian are presented in Sec. IV.

The form of the GLE in Eq. (18), which is local in space, is not the most general form and it represents an approximation to the dynamical equations. The exact dynamical equations can be formally recast in terms of a chain of GLE equations for successive random forces involving nonlocal memory functions that are correlation functions of appropriate random forces.[31,46] The version of the GLE presented above is obtained by truncating this chain and by replacing the memory function by an approximate, constant, friction tensor. This GLE is local in space and the constant friction tensor is evaluated at a single characteristic configuration of the system, the configuration at the saddle point. Because we have chosen a simplified version of a GLE to describe the dynamics, the effective Hamiltonian in Eq. (22) only involves linear couplings between the system and the bath. One may consider the same form for the effective Hamiltonian with harmonic bath coordinates but allowing for nonlinear coupling between the system and the bath. In this case a nonlinear GLE equation for the dynamics results.[25,39,47]

Even more complicated representations for the dynamics can be considered by introducing higher order couplings and anharmonic terms in the Hamiltonian, Eq. (22). The construction of less approximate effective Hamiltonians and the specification of higher order terms are open research problems that are beyond the scope of the current work. The precise conditions under which one can reduce the solvent dynamics to this simple form of the GLE are not generally known. The validity of approximating a local friction tensor by a constant one for the proton transfer reaction studied here could be investigated by evaluating the friction tensor with the system fixed at other configurations. The reaction considered here has a highly peaked barrier, so a local region around the saddle point determines the fate of a dynamical trajectory. Because of this feature, the solute dynamics near the saddle point will be fast compared to the solute response and approximating the local friction tensor by a constant at the saddle point will give a good representation of the dynamics.

It is well known that solvents are not harmonic, and solute-solvent coupling is not bilinear and in fact is strongly nonlinear. However, generalized Langevin theory in the form given in Eqs. (18) and (22) may be applied when one can identify suitable variables associated with the solvent that *act* as effective oscillators, as discussed by Hynes and co-workers.[48,49] Evidence for the validity of the local, linear approximation to the solvent friction is also offered by the general success of Grote-Hynes theory[50] and more generally the linear response approximation. The GLE in Eq. (18) is the basis for the Grote-Hynes friction correction to TST. Furthermore, the Grote-Hynes friction correction can be derived by applying variational transition state theory (VTST) to the effective Hamiltonian in Eq. (18) with a locally quadratic potential.[23,51] The validity of the Grote-Hynes method, and the underlying Hamiltonian, for a variety of model reactions has been confirmed by comparing results from Grote-Hynes theory with accurate classical simulations of the reaction dynamics.[49,52] Similar tests of the validity of the effective GLE Hamiltonian in Eq. (22) for the proton transfer reaction studied here are planned for future studies.

III.B. Variational transition state theory

The starting point for the VTST/MT calculations is the GLE Hamiltonian in Eq. (22) from which we identify the effective potential

$$V_{\rm eff}^{\rm NES}(z_{\rm A},z_{\rm B},z_{\rm H},y_1,\ldots,y_N) = W(r,R)+\sum_{j=1}^{N}\frac{1}{2}m_b\omega_j^2\left(y_j-\sum_{\alpha={\rm A,B,H}}C_{j\alpha}z_\alpha\right)^2, \tag{26}$$

where Eq. (17) provides the relationship between r, R and $z_{\rm A},z_{\rm B},z_{\rm H}$. The application of variational transition state theory to this form of potential is described in detail elsewhere.[10,23–27] For convenience, a brief overview of the approach is provided here.

III.B.1. Equilibrium solvation

An equilibrium solvation (ES) model is recovered from the GLE Hamiltonian if the potential is minimized with respect to the bath coordinates for each choice of solute coordinates, i.e.,

$$y_j^{\rm ES}(z_{\rm A},z_{\rm B},z_{\rm H}) = \sum_{\alpha={\rm A,B,H}} C_{j\alpha}z_\alpha, \tag{27}$$

and the resulting equilibrium solvation potential is the PMF, i.e., $V_{\rm eff}^{\rm ES}=W(r,R)$. The saddle point on the PMF is defined by $r^\ddagger$ and $R^\ddagger$ and the choice of $Z_{\rm CM}$ is arbitrary, so we choose it to be zero for convenience. The minimum energy path on the PMF is obtained by following the paths of steepest descent from the saddle point toward reactants and products in a mass-scaled coordinate system in which the reduced mass of each coordinate is the same. We call this the equilibrium solvation path (ESP), $z_\alpha^{\rm ES}(s_{\rm ES})$, where the reaction coordinate $s_{\rm ES}$ is the signed distance from the saddle point along the curvilinear ESP through the mass-scaled coordinate system and is negative on the reactant side. Generalized transition-state dividing surfaces in the equilibrium solvation model are defined to be orthogonal to the ESP, and the transition-state theory approximation to the reaction rate is obtained from the net flux toward products through the dividing surface.[18–20] In a classical world this dynamical approximation causes an overestimate of the rate constant which is the basis for variationally optimizing the location of the dividing surface (along the reaction coordinate) to minimize the rate constant.[17,20,53] With this approximation the expression for the generalized transition-state-theory (GT) rate constant reduces to[21,54]

$$k_{\rm ES}^{\rm GT}(T,s_{\rm ES}) = \frac{k_{\rm B}T}{hQ^{\rm R}(T)}Q_{\rm ES}^{\rm GT}(T,s_{\rm ES})\exp\left[-\frac{V_{\rm ESP}(s_{\rm ES})}{k_{\rm B}T}\right], \tag{28}$$

where h is Planck's constant, $Q^{\rm R}(T)$ is the reactant partition function for a unimolecular reaction or the reactant partition function per unit volume for a bimolecular reaction, $Q_{\rm ES}^{\rm GT}(T,s_{\rm ES})$ is the generalized transition-state partition function for the bound modes orthogonal to the reaction path at $s_{\rm ES}$, and $V_{\rm ESP}(s_{\rm ES})$ is the value of the PMF evaluated on the ESP at $s_{\rm ES}$

$$\begin{aligned}V_{\rm ESP}(s_{\rm ES}) &= V_{\rm eff}^{\rm NES}[z_{\rm A}^{\rm ES}(s_{\rm ES}),z_{\rm B}^{\rm ES}(s_{\rm ES}),z_{\rm H}^{\rm ES}(s_{\rm ES}),\\ &\qquad y_1^{\rm ES}(s_{\rm ES})\cdots,y_N^{\rm ES}(s_{\rm ES})]\\ &= W[r(s_{\rm ES}),R(s_{\rm ES})].\end{aligned} \tag{29}$$

The present application, Eq. (1), is a unimolecular reaction so we will specialize to that case. Conventional transition-state theory (TST) is recovered by evaluating Eq. (28) at $s_{\rm ES}=0$, which yields

$$k_{\rm ES}^{\rm TST}(T)=k_{\rm ES}^{\rm GT}(T,s_{\rm ES}=0) \tag{30}$$

and canonical variational theory (CVT) is obtained by minimizing Eq. (28) with respect to $s_{\rm ES}$

$$k_{\rm ES}^{\rm CVT}(T)=\min_{s_{\rm ES}} k_{\rm ES}^{\rm GT}(T,s_{\rm ES}). \tag{31}$$

Partition functions are computed quantum mechanically within the harmonic approximation:

$$Q^{\mathrm{R}}(T)=\prod_{m=1}^{N+2}\frac{1}{2\sinh[\hbar\omega_m^{\mathrm{R}}/2k_{\mathrm{B}}T]}$$
$$=\prod_{m=1}^{2}\frac{1}{2\sinh[\hbar\omega_m^{\mathrm{R,AHB}}/2k_{\mathrm{B}}T]}$$
$$\times\prod_{j=1}^{N}\frac{1}{2\sinh[\hbar\omega_j/2k_{\mathrm{B}}T]}, \tag{32}$$

$$Q_{\mathrm{ES}}^{\mathrm{GT}}(T,s_{\mathrm{ES}})=\prod_{m=1}^{N+1}\frac{1}{2\sinh[\hbar\omega_m^{\mathrm{ES}}(s_{\mathrm{ES}})/2k_{\mathrm{B}}T]}$$
$$=\frac{1}{2\sinh[\hbar\omega_1^{\mathrm{ES}}(s_{\mathrm{ES}})/2k_{\mathrm{B}}T]}$$
$$\times\prod_{j=1}^{N}\frac{1}{2\sinh[\hbar\omega_j/2k_{\mathrm{B}}T]}, \tag{33}$$

where $\hbar\equiv h/2\pi$. In the equilibrium solvation model the bath modes decouple from the solute modes; this decoupling is explicitly indicated in Eqs. (32) and (33). Normal modes for the solute frequencies at reactants and the saddle point are obtained by diagonalizing the 3×3 Hessian matrix in the $(z_{\mathrm{A}},z_{\mathrm{B}},z_{\mathrm{H}})$ coordinates. Generalized normal modes (which are the vibrational modes at locations were the gradient is not zero) are obtained by first projecting out the gradient vector from the Hessian matrix, then diagonalizing the projected Hessian matrix.[55] One mode has a zero frequency corresponding to the center-of-mass translation. This mode is omitted from both the reactant and generalized transition-state partition functions. At reactants there are two bound frequencies (corresponding approximately to proton vibration and A–B vibration) while along the reaction path one mode corresponds to the unbound reaction coordinate motion. Therefore there are two solute modes in the reactant partition function and only one in the generalized transition-state partition function. In the equilibrium solvation mode, contributions from the N bath modes cancel in the reactant and transition-state partition functions.

Quantum mechanical effects on reaction coordinate motion are included by a multiplicative transmission coefficient[54]

$$k_{\mathrm{ES}}^{\mathrm{CVT}/t}(T)=\kappa_{\mathrm{ES}}^{t}(T)k_{\mathrm{ES}}^{\mathrm{CVT}}(T). \tag{34}$$

Multidimensional tunneling effects are included by the zero-order canonical mean shape (CMS-0) approximation.[10] Probabilities are computed semiclassically for transmission by the one-dimensional CMS-0 potential, which in the harmonic approximation is given by

$$V_{\mathrm{ES}}^{\mathrm{CMS}-0}(s_{\mathrm{ES}})=V_{\mathrm{ESP}}(s_{\mathrm{ES}})+\frac{\hbar}{2}\sum_{m=1}^{N+1}\omega_m^{\mathrm{ES}}(s_{\mathrm{ES}}). \tag{35}$$

Although the CMS-0 potential is a one-dimensional function of the reaction coordinate, multidimensional effects are included in two ways. First, $V_{\mathrm{ES}}^{\mathrm{CMS-0}}(s_{\mathrm{ES}})$ depends on the orthogonal modes because of the sum in Eq. (35). Second, we use an effective reduced mass that corresponds to an effective tunneling path in the multidimensional space.[56] The effective tunneling path differs from the ESP because the ESP is curved. In this work we use the centrifugal-dominant small-curvature tunneling method[57,58] (denoted SCT) that includes the effects of reaction-path curvature by means of an effective reduced mass. The effective reduced mass is smaller than the common reduced mass introduced below Eq. (27), and this accounts for the increased probability of tunneling along corner-cutting paths on the concave side of the ESP.[57,58] The reaction probabilities $P_{\mathrm{ES}}^{\mathrm{SCT}}(E)$ are thermally averaged and normalized by the thermal average of the reaction probabilities corresponding to zero-curvature classical reaction coordinate motion[10] on the potential of Eq. (35) to give the transmission coefficient $\kappa_{\mathrm{ES}}^{\mathrm{SCT}}(T)$

$$\kappa_{\mathrm{ES}}^{\mathrm{SCT}}(T)=\frac{\int_0^\infty dE e^{-\beta E}P_{\mathrm{ES}}^{\mathrm{SCT}}(E)}{\int_0^\infty dE e^{-\beta E}\theta\left[E-\max_{s_{\mathrm{ES}}}V_{\mathrm{ES}}^{\mathrm{CMS}-0}(s_{\mathrm{ES}})\right]}, \tag{36}$$

where $\theta(x)$ is the Heaviside step function $[\theta(x)=0,\ x<0;\theta(x)=1,x>0]$. We also compute tunneling with the zero-curvature tunneling (ZCT) approximation in which the effects of reaction-path curvature are neglected so that the effective reduced mass[57,58] is equal to the common reduced mass used in the ESP calculations described below Eq. (27).

III.B.2. Nonequilibrium solvation

The saddle point geometry on the effective potential in Eq. (26) is at $(z_{\mathrm{A}}^{\ddagger},z_{\mathrm{B}}^{\ddagger},z_{\mathrm{H}}^{\ddagger},y_1^{\ddagger},\cdots,y_N^{\ddagger})$ where

$$\begin{pmatrix} z_{\mathrm{A}}^{\ddagger}\\ z_{\mathrm{B}}^{\ddagger}\\ z_{\mathrm{H}}^{\ddagger}\end{pmatrix}=\mathbf{A}^{-1}\begin{pmatrix} r^{\ddagger}\\ R^{\ddagger}\\ Z_{\mathrm{CM}}=0\end{pmatrix}, \tag{37}$$

$$y_j^{\ddagger}=\sum_{\alpha=\mathrm{A,B,H}}C_{j\alpha}z_\alpha^{\ddagger}, \tag{38}$$

so that at the saddle point for the full system, the geometry corresponds to the saddle point on the equilibrium solvation path. The minimum energy path on the effective potential is obtained by following the paths of steepest descent from the saddle point toward reactants and products in a mass-scaled coordinate system including both solute and bath coordinates in which the mass of each coordinate is the same. We call this the nonequilibrium solvation path (NESP), $z_\alpha^{\mathrm{NES}}(s_{\mathrm{NES}}),y_j^{\mathrm{NES}}(s_{\mathrm{NES}})$, where the new reaction coordinate s_{NES} is the signed distance from the saddle point along the curvilinear NESP and is negative on the reactant side. Generalized transition-state dividing surfaces in the nonequilibrium solvation model are defined to be orthogonal to the NESP and the rate constant expression is similar to Eq. (28); however, the superscript ES is replaced by NES to indicate that the potential along the reaction path, $W_{\mathrm{NESP}}(s_{\mathrm{NES}})$, and the partition functions for bound modes orthogonal to the NESP, $Q_{\mathrm{NES}}^{\mathrm{GT}}(T,s_{\mathrm{NES}})$, are different than in the equilibrium solvation model. The potential along the NESP is given by

$$V_{\mathrm{NESP}}(s_{\mathrm{NES}}) = V_{\mathrm{eff}}^{\mathrm{NES}}[z_{\mathrm{A}}^{\mathrm{NES}}(s_{\mathrm{NES}}), z_{\mathrm{B}}^{\mathrm{NES}}(s_{\mathrm{NES}}), z_{\mathrm{H}}^{\mathrm{NES}}(s_{\mathrm{NES}}), y_1^{\mathrm{NES}}(s_{\mathrm{NES}}), \cdots, y_N^{\mathrm{NES}}(s_{\mathrm{NES}})], \tag{39}$$

and the generalized transition-state partition function is written

$$Q_{\mathrm{NES}}^{\mathrm{GT}}(T, s_{\mathrm{NES}}) = \prod_{m=1}^{N+1} \frac{1}{2\sinh[\hbar\omega_m^{\mathrm{NES}}(s_{\mathrm{NES}})/2k_{\mathrm{B}}T]}, \tag{40}$$

where the frequencies are obtained by diagonalizing the $(N+3)\times(N+3)$ mass-weighted Hessian matrix [obtained from the second derivatives of the potential in Eq. (26)] with the gradient projected out. The form of Eq. (26) still gives rise to a zero frequency mode that transforms like the center-of-mass motion of the solute with

$$\Delta y_j^0 = \sum_{\alpha=\mathrm{A,B,H}} C_{j\alpha} m_\alpha \Delta Z_{\mathrm{CM}}. \tag{41}$$

This mode is omitted from Eq. (40) as well as the mode that corresponds to motion along the reaction coordinate. Since the bath modes represent nonequilibrium solvation effects near the saddle point, the coupling between the bath and solute should not be included in the (equilibrium) reactant partition function. Therefore, Eq. (32) gives the expression for the reactant partition function in both the equilibrium and nonequilibrium solvation models.

Since the effective potential at the saddle point in the nonequilibrium solvation model is the same as that in the equilibrium solvation model, the nonequilibrium conventional TST rate constant is related to the equilibrium one by

$$k_{\mathrm{NES}}^{\ddagger}(T) = \frac{Q_{\mathrm{NES}}^{\ddagger}(T)}{Q_{\mathrm{ES}}^{\ddagger}(T)} k_{\mathrm{ES}}^{\ddagger}(T), \tag{42}$$

where the transition-state partition functions are given by Eqs. (33) and (40) with the reaction coordinate set to zero. Note that even though the saddle point geometry and effective potential are the same in the two models, the harmonic frequencies are not in general, since the nonequilibrium solvation model includes coupling between the bath and solute modes that is neglected in the equilibrium solvation model. (However, this coupling is not included in the reactant partition functions since by definition the reactant is at equilibrium.) The GLE in Eq. (18) is the basis for the Grote-Hynes[50] friction correction to TST, which results from nonequilibrium solvation. In the Grote-Hynes approach the reaction dynamics are treated classically and the PMF is approximated by a quadratic expansion about the saddle point. With these approximations the ratio of partition functions in Eq. (42) can be written

$$\frac{Q_{\mathrm{NES}}^{\ddagger}(T)}{Q_{\mathrm{ES}}^{\ddagger}(T)} \xrightarrow[\text{classical limit}]{} \prod_{m=1}^{N+1} \frac{\omega_m^{\mathrm{NES}}(s_{\mathrm{ES}}=0)}{\omega_m^{\mathrm{NES}}(s_{\mathrm{NES}}=0)}, \tag{43}$$

and this expression is recognized as the Grote-Hynes correction factor.[50,51] In the approach used in this paper we do not constrain the transition-state dividing surface to be located at the saddle point; furthermore, we treat the partition functions quantum mechanically. In addition, quantum mechanical effects on reaction coordinate motion are also treated by using the SCT method as described above. The CMS-0 potential in the nonequilibrium solvation model is similar to Eq. (35), but the bound frequencies along the nonequilibrium solvation path are different from those in the equilibrium solvation model. Furthermore, the nonequilibrium solvation path can include curvature coupling from the bath modes that are not included in the equilibrium solvation model.

IV. CALCULATION DETAILS

All calculations in this study were carried out at 249 K. Molecular dynamics simulation calculations were performed on this model system in order to acquire the data necessary as input for the VTST/MT rate calculation, namely, the potential of mean force $W(r,R)$ and the force–force time correlation functions used to define the friction tensor $\boldsymbol{\eta}(t)$. For the purposes of this study, the values of the internal coordinates r and R in the reactive complex were kept constant throughout each MD simulation. This allows the calculation of average forces on definite ''clamped'' values of the internal coordinates.

The molecular dynamics calculations were performed under very similar conditions to those reported by Azzouz and Borgis[7] and Hammes-Schiffer and Tully.[9] The simulations were performed using periodic boundary conditions on 250 methyl chloride molecules and one reactive complex in a truncated octahedron with a number density of $\rho = 0.012\ \text{Å}^{-3}$ at $T = 249\ \text{K}$, a temperature enforced by the use of a Nosé thermostat.[59] The Lennard-Jones potentials between the sites (Cl atoms or CH_3 groups) of one solvent molecule and those of another and between sites of solvent molecules and sites of the solute were spherically truncated at $R_c = 13.8\ \text{Å}$, and shifted to make them continuous. The Coulombic interactions between all molecules were also smoothly and spherically truncated at $R_c = 13.8\ \text{Å}$ with the same Steinhauser truncation function, $T(R_{ij})$, used by Hammes-Schiffer and Tully,[9] reproduced here for convenience:

$$T(R_{ij}) = \begin{cases} 1 & R_{ij} \leqslant R_T \\ 1 - \dfrac{(R_{ij}-R_T)^2(3R_c - R_T - 2R_{ij})}{(R_c - R_T)^3} & R_T \leqslant R_{ij} \leqslant R_c, \\ 0 & R_{ij} \geqslant R_c \end{cases} \tag{44}$$

where R_{ij} is the distance between the centers of two interacting molecules and $R_T = 0.95R_c$. The equations of motion were integrated using a velocity-Verlet algorithm for the translations and a leapfrog algorithm with Lagrange multiplier for the rotations.[60] The integration time step was 0.1 fs, which kept total energy fluctuations to within a relative standard deviation of approximately 0.01% during the course of a typical 50 ps run.

Hammes-Schiffer and Tully provided us with their own calculations of the potential of mean force, and the two sets of results are in excellent agreement.

IV.A. Potential of mean force

Using the Hamiltonian in Eq. (9) and the transformation in Eq. (17), the potential of mean force, $W(r,R)$, which is defined by Eq. (19), can be expressed in the r,R coordinates by

$$\frac{\partial W}{\partial r}=\left\langle\frac{\partial H}{\partial r}\right\rangle_{r,R}=\frac{\partial V_{\mathrm{HB}}}{\partial r}+\frac{\partial W_{\mathrm{S}}}{\partial r}+\left\langle\frac{\partial}{\partial r}\left[\frac{1}{2I(r,R)}\left(P_\theta^2+\frac{P_\phi^2}{\sin^2\theta}\right)\right]\right\rangle_{r,R}=\frac{\partial V_{\mathrm{HB}}}{\partial r}+\frac{\partial W_{\mathrm{S}}}{\partial r}-k_{\mathrm{B}}T\frac{\partial \ln I(r,R)}{\partial r} \tag{45}$$

and

$$\frac{\partial W}{\partial R}=\left\langle\frac{\partial H}{\partial R}\right\rangle_{r,R}=\frac{\partial V_{\mathrm{HB}}}{\partial R}+\frac{\partial W_{\mathrm{S}}}{\partial R}+\left\langle\frac{\partial}{\partial_R}\left[\frac{1}{2I(r,R)}\left(P_\theta^2+\frac{P_\phi^2}{\sin^2\theta}\right)\right]\right\rangle_{r,R}=\frac{\partial V_{\mathrm{HB}}}{\partial R}+\frac{\partial W_{\mathrm{S}}}{\partial R}-k_{\mathrm{B}}T\frac{\partial \ln I(r,R)}{\partial R}, \tag{46}$$

where the averaging is done over all variables in the Hamiltonian other than r, R, and Z_{CM}. A brief derivation of the last terms in the second lines of Eqs. (45) and (46) is provided in Appendix A. If the moment of inertia is approximated by $\mu_{\mathrm{AB}}R^2$, then the last term in Eq. (45) vanishes and the last term in Eq. (46) reduces to the usual expression $2k_{\mathrm{B}}T/R$.[61] The partial derivatives of the potential of mean force due to the direct solvent interactions, W_{S}, are given by

$$\frac{\partial W_{\mathrm{S}}}{\partial r}\equiv\left\langle\frac{\partial V_{\mathrm{CS}}}{\partial r}\right\rangle_{r,R} \tag{47}$$

and

$$\frac{\partial W_{\mathrm{S}}}{\partial R}\equiv\left\langle\frac{\partial V_{\mathrm{CS}}}{\partial R}\right\rangle_{r,R}. \tag{48}$$

Integrating Eqs. (45) and (46), the potential of mean force can be written

$$W(r,R)=W_0+V_{\mathrm{HB}}(r,R)+W_{\mathrm{S}}(r,R)-k_{\mathrm{B}}T\ln\left[\frac{I(r,R)}{I(r_0,R_0)}\right], \tag{49}$$

where W_0, r_0, and R_0 are arbitrary constants of integration. We set R_0 equal to 2.70 Å, and we set W_0 such that $W(r,R)$ equals 0 at the minimum of the reactant well. The calculations presented below do not depend explicitly on the constant r_0, so it is left arbitrary. Operationally, the solvent free energy, W_{S}, can be calculated from numerical integration of its derivatives in Eqs. (47) and (48). In practice, Azzouz and Borgis[7] have found that $\partial V_{\mathrm{CS}}/\partial R$ is nearly constant in the range $2.5\,\text{Å}<R<3.0\,\text{Å}$, so that the solvent free energy in this range of R can be accurately approximated by

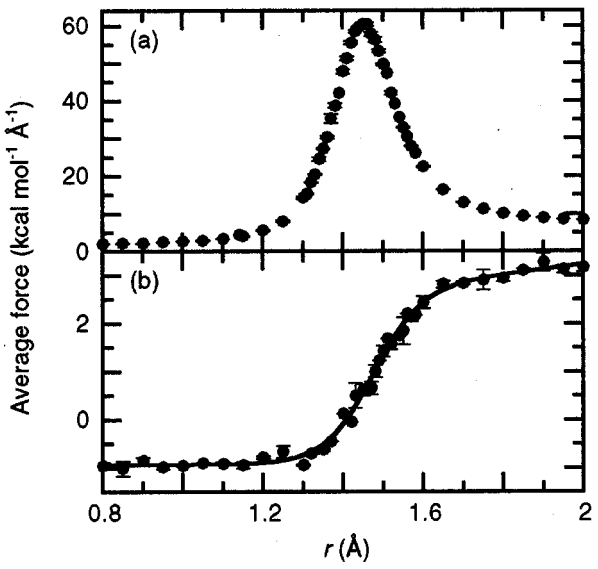

FIG. 1. Average external forces (a) $-\langle\partial V_{\mathrm{CS}}/\partial r\rangle_{r,R}$ and (b) $-\langle\partial V_{\mathrm{CS}}/\partial R\rangle_{r,R}$, as a function of r for fixed $R=2.70$ Å [see Eqs. (43) and (44)]. Solid circles are the data obtained from molecular dynamics simulations, and error bars indicate statistical uncertainty at representative points. The curve in part (b) is a fit to the functional form in Eq. (53).

$$W(r,R)=W_0+V_{\mathrm{HB}}(r,R)+A(r)-B(r)(R-R_0)-2k_{\mathrm{B}}T\ln(R/R_0), \tag{50}$$

where we have used the approximation $I\cong\mu_{\mathrm{AB}}R^2$,

$$A(r)=\int_{r_0}^{r}dr'\left\langle\frac{\partial V_{\mathrm{CS}}}{\partial r}\right\rangle_{r=r',R=R_0} \tag{51}$$

and

$$B(r)=-\left\langle\frac{\partial V_{\mathrm{CS}}}{\partial R}\right\rangle_{r,R=R_0}. \tag{52}$$

The averages in Eqs. (51) and (52) were calculated as functions of r by performing individual MD simulations for values of r in regularly spaced 0.05 Å intervals ranging from 0.8 to 1.3 Å and from 1.6 to 2.0 Å, all for a fixed value of $R_0=2.7$ Å. A finer grid of averages, spaced at 0.02–0.03 Å intervals, was calculated from $r=1.3$ to 1.6 Å since the average force on the r coordinate is sharply peaked in this interval. The total simulation time at each value of r was at least 50 ps; in the range $r=1.30$ to 1.50 Å, several independent 50 ps calculations were averaged. Figure 1 shows these average external forces as a function of r for a fixed R equal to 2.70 Å.

After these average external forces were calculated, $A(r)$ was calculated by evaluating the integral in Eq. (51) with a trapezoid rule, using $r_0=0.8$ Å and $R_0=2.7$ Å. Then smooth functions $f_{\mathrm{A}}(r)$ and $f_{\mathrm{B}}(r)$ were fitted to the numerically determined values of $A(r)$ and $B(r)$, where each of the smooth functions is of the form

$$f(r)=a_1\left(\frac{e^{a_3(r-a_2)}-e^{-a_4(r-a_2)}}{e^{a_5(r-a_2)}+e^{-a_6(r-a_2)}}\right)+a_7, \tag{53}$$

TABLE III. Nonlinear fit parameters.[a]

	$A(r)$	$B(r)$
a_1	−6.250 827	1.929 821
a_2	1.452 337	1.465 449 5
a_3	9.150 984	6.003 337
a_4	9.148 94	10.318 115
a_5	8.143	5.663 757
a_6	8.799 735	10.561 206
a_7	−7.814 075	0.903 583

[a]Units are such that coordinates in Å yield $A(r)$ in units of kcal/mol and $B(r)$ in units of kcal mol^{-1} Å^{-1}.

which is chosen solely for its numerical flexibility. The best-fit parameters for this functional form were found via a quasi-Newton nonlinear fitting algorithm, and are given in Table III. Figure 2 shows these functions along with the data points to which the fit was performed. A contour plot of the resulting potential and plots of the potential along cuts with $R=2.6265$ Å (the value of R at the saddle point) and $R=2.70$ Å (the value of R near the reactant and product minima) are shown in Fig. 3.

IV.B. Force–force correlation function

The other simulation-produced information needed as input for the rate constant calculation is the friction kernel of the generalized Langevin equation. This kernel is obtained from calculations of force–force time correlation functions as shown in Eq. (20). Rather than calculate the correlation functions for the fluctuations in force for the coordinates $\mathbf{z}=(z_A,z_B,z_H)$, as indicated in Eq. (21), we calculate the correlation functions in the Cartesian coordinates $(\mathbf{r}_A,\mathbf{r}_B,\mathbf{r}_H)$ then transform back to the $\mathbf{z}$ coordinates. To accomplish this, we first define force vectors in the Cartesian coordinates by gradients of H:

$$\mathbf{F}_\alpha=-\frac{\partial H}{\partial \mathbf{r}_\alpha}=-\frac{\partial V_{\mathrm{HB}}}{\partial \mathbf{r}_\alpha}-\frac{\partial V_{\mathrm{CS}}}{\partial \mathbf{r}_\alpha},\quad \alpha=\mathrm{A,B,H}, \tag{54}$$

where $\partial/\partial\mathbf{r}_\alpha$ is a gradient vector, and the fluctuations in force are given by

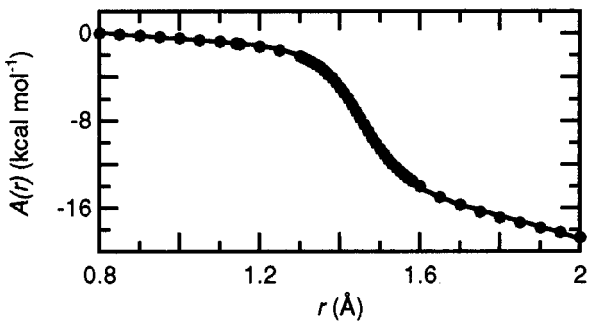

FIG. 2. Function $A(r)$ used to fit the potential of mean force $W(r,R)$ [see Eq. (50)] and obtained by integrating $\langle \partial V_{\mathrm{CS}}/\partial r\rangle_{r,R}$ from 0.8 Å to r. Solid circles are the data obtained from numerical integration of the data points shown in Fig. 1. The curve is a fit to the functional form in Eq. (53).

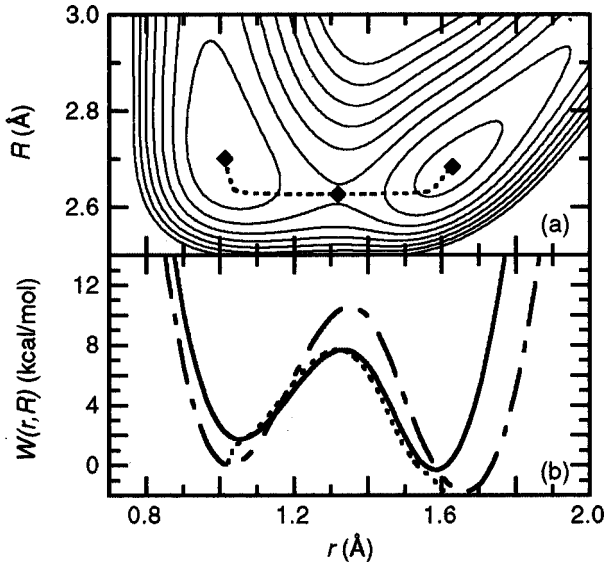

FIG. 3. (a) Equipotential contours of the potential of mean force $W(r,R)$. Contours (solid curves) are plotted for energies of 0, 4, 8, 12, 16, 20, 24, and 28 kcal/mol. The zero of energy is taken as the minimum of the reactant well at $r=1.01$ Å, $R=2.70$ Å. The solid diamonds indicate the locations of the reactant and product minimum and the saddle point. The dashed curve depicts the minimum energy path. (b) Potential $W(r,R)$ as a function of r for R fixed at 2.6265 Å (solid curve), for R fixed at 2.7 Å (chain curve), and along the minimum energy path (dotted curve).

$$\delta\mathbf{F}_\alpha(t)\equiv\mathbf{F}_\alpha(t)-\langle\mathbf{F}_\alpha\rangle_{r,R}=-\frac{\partial V_{\mathrm{CS}}}{\partial\mathbf{r}_\alpha}(t)+\left\langle\frac{\partial V_{\mathrm{CS}}}{\partial\mathbf{r}_\alpha}\right\rangle_{r,R},$$

$$\alpha=\mathrm{A,B,H}. \tag{55}$$

(Note that V_{HB} is a function of only $\mathbf{z}$ so that the difference of the instantaneous and averaged values of its gradients vanishes.) The force component fluctuations in the $\mathbf{z}$ coordinates, as shown in Eq. (21), are then given in terms of the force vector fluctuations in the Cartesian coordinates by

$$\delta F_\alpha(t)=\hat{\mathbf{z}}\cdot\delta\mathbf{F}_\alpha(t),\quad \alpha=\mathrm{A,B,H}. \tag{56}$$

The 3×3 block $\boldsymbol{\eta}^{(\mathbf{r})}_{\alpha\alpha'}(t)$ of the 9×9 friction tensor in the Cartesian coordinates $(\mathbf{r}_A,\mathbf{r}_B,\mathbf{r}_H)$ for $\mathbf{r}_\alpha$ and $\mathbf{r}_{\alpha'}$ is given in terms of the correlation functions between force fluctuations on Cartesian coordinates $\mathbf{r}_\alpha$ and $\mathbf{r}_{\alpha'}$ by

$$\begin{aligned}k_{\mathrm{B}}T\boldsymbol{\eta}^{(\mathbf{r})}_{\alpha\alpha'}(t)&=\langle\delta\mathbf{F}_\alpha(t)\,\delta\mathbf{F}_{\alpha'}(0)\rangle_{r,R}\\&=\langle[\mathbf{F}_\alpha(t)-\langle\mathbf{F}_\alpha\rangle_{\mathbf{z}}][\mathbf{F}_{\alpha'}(0)-\langle\mathbf{F}_{\alpha'}\rangle_{\mathbf{z}}]\rangle_{r,R}\\&=\langle\mathbf{F}_\alpha(t)\mathbf{F}_{\alpha'}(0)\rangle_{r,R}-\langle\mathbf{F}_\alpha\rangle_{r,R}\langle\mathbf{F}_{\alpha'}\rangle_{r,R}.\end{aligned} \tag{57}$$

When calculating the correlation functions from a finite, discrete set of force data, the averages in Eq. (57) are carried out over a slightly different set of data for each value of t. For a run with N_t total time steps of size Δt, one estimate of the nth discrete value of the friction tensor is given by

$$
\begin{aligned}
k_B T \boldsymbol{\eta}^{(\mathbf{r})}_{\alpha\alpha'}(n\Delta t) &= \frac{1}{(N_t-n)} \sum_{n'=1}^{N_t-n} [\delta\mathbf{F}_\alpha((n+n')\Delta t)\,\delta\mathbf{F}_{\alpha'}(n'\Delta t)] \\
&= \frac{1}{(N_t-n)} \sum_{n'=1}^{N_t-n} [\mathbf{F}_\alpha((n+n')\Delta t)\mathbf{F}_{\alpha'}(n'\Delta t) \\
&\quad -\mathbf{F}_\alpha((n+n')\Delta t)\langle\mathbf{F}_{\alpha'}\rangle_{r,R} \\
&\quad -\langle\mathbf{F}_\alpha\rangle_{r,R}\mathbf{F}_{\alpha'}(m'\Delta t)+\langle\mathbf{F}_\alpha\rangle_{r,R}\langle\mathbf{F}_{\alpha'}\rangle_{r,R}], \qquad (58)
\end{aligned}
$$

where

$$
\langle\mathbf{F}_\alpha\rangle_{r,R}=\frac{1}{N_t}\sum_{n=1}^{N_t}\mathbf{F}_\alpha(n\Delta t). \qquad (59)
$$

A second estimate of this value of the friction tensor is obtained using the last expression in Eq. (57) to give

$$
\begin{aligned}
k_B T \boldsymbol{\eta}^{(\mathbf{r})}_{\alpha\alpha'}(n\Delta t) &= \frac{1}{(N_t-n)} \sum_{n'=1}^{N_t-n} \mathbf{F}_\alpha((n+n')\Delta t)\mathbf{F}_{\alpha'}(n'\Delta t) \\
&\quad -\langle\mathbf{F}_\alpha\rangle_{r,R}\langle\mathbf{F}_{\alpha'}\rangle_{r,R}. \qquad (60)
\end{aligned}
$$

Comparison of results using Eqs. (58) and (60) provides a self-consistency check of the numerical uncertainty in the computed friction tensors. We found that they agree to within the numerical errors. The 3×3 friction tensor in the **z** coordinates is obtained by transforming each 3×3 block of the 9×9 friction tensor in Cartesian coordinates by using Eq. (56) to get the single component along the A–B bond for each atom, A, B, and H.

The friction kernel at the saddle point in the **z** coordinates is fitted with a finite sum of cosines in the same manner as in our previous work.[23,27] Each element $\eta_{\alpha\alpha'}$ is expanded in a finite cosine series:

$$
\eta_{\alpha\alpha'}(t)\approx\sum_{L=0}^{N_C}\eta_{L\alpha\alpha'}\cos(\omega_L t), \qquad (61)
$$

where N_C+1 is the number of cosines used in the fit, the expansion coefficients $\eta_{L\alpha\alpha'}$ are given by

$$
\eta_{L\alpha\alpha'}=\frac{2}{t_C}\int_0^{t_C}\cos(\omega_L t)\,\eta_{\alpha\alpha'}(t)dt, \qquad (62)
$$

and t_C is the cutoff time for the cosine expansion fit. Several of the components of the friction tensor have significant long-time decays. Since the cosine expansion method described here works best when the function being fitted goes to zero at $t=t_C$, these long time, "static friction" parts of the friction components are included approximately by including the very low frequency ω_0. The final results of the calculation are not particularly sensitive to the value of ω_0, so we have set it equal to 1/8 the value of ω_1 in Eq. (63). With this choice for ω_0, the frequencies are given by

$$
\omega_0=\frac{\pi}{16t_C},
$$

$$
\omega_L=\frac{\pi}{t_C}\left(L-\frac{1}{2}\right),\quad L=1,\ldots,N_C. \qquad (63)
$$

Since $\boldsymbol{\eta}$ is a symmetric matrix, each L block of $\eta_{L\alpha\alpha'}$ is also symmetric and thus can be diagonalized

$$
\eta_{L\alpha\alpha'}=\sum_{\alpha''=\mathrm{A,B,H}}U_{L\alpha\alpha''}\lambda_{L\alpha''}U_{L\alpha'\alpha''}, \qquad (64)
$$

where $\lambda_{L\alpha}$ are the eigenvalues and the corresponding eigenvectors $\mathbf{U}_L$ are orthonormal. Equation (61) then becomes

$$
\eta_{\alpha\alpha'}(t)\approx\sum_{L=0}^{N_C}\sum_{\alpha''=\mathrm{A,B,H}}U_{L\alpha\alpha''}\lambda_{L\alpha''}U_{L\alpha'\alpha''}\cos(\omega_L t). \qquad (65)
$$

This can be rearranged into a single summation by associating a single index j with the dual index $(L\alpha)$ and changing the summation limits appropriately

$$
\eta_{\alpha\alpha'}(t)\approx\sum_{j=1}^{3(N_C+1)}U_{j\alpha}\lambda_j U_{j\alpha'}\cos(\omega_j t). \qquad (66)
$$

Equating this result with Eq. (23) with $N=3(N_C+1)$ determines coupling constants of the GLE Hamiltonian, Eq. (22), on which the VTST calculations are based, namely,

$$
C_{j\alpha\alpha'}=\frac{U_{L\alpha\alpha'}}{\omega_L}\sqrt{\frac{\lambda_{L\alpha'}}{m_b}}. \qquad (67)
$$

By using this procedure, each of the N_C+1 frequencies in Eq. (61) is coupled separately to each degree of freedom in the reactive complex in Eq. (18).

The cutoff time for the fit, t_C, is chosen so that all of the elements of the friction function matrix are close to zero at t_C. The results are not overly sensitive to t_C, varying by only 4% when t_C is varied from 1.5 to 2.5 ps. For the final calculations we set $t_C=2.25$ ps. As was the case in our previous work,[27] using $N_C=5$ provides a fit of adequate quality over the short time scale relevant to the reaction dynamics. A comparison between the elements of the friction matrix and the fits with $N_C=5$ (i.e., with six cosine terms) is given in Fig. 4. The recurrences seen in Fig. 4 are a consequence of the periodicity inherent in Eq. (61). The recurrence time is determined by the choice of t_C. With our choice of t_C, the nonphysical recurrence in the fit occurs on a time scale too long to significantly influence the calculated rate constants

IV.C. VTST/MT calculation

Once the simulation calculations have been completed, the processed data are used as input for the semiclassical VTST/MT calculations. Specifically, the minimum energy path (MEP) is determined by following the negative gradient of the potential surface (in mass-scaled coordinates), and the signed reaction-path distance, s, is calculated by integrating the arc length along this path in both the reactant (negative s) and product (positive s) directions. The former is done using an Euler integrator[62] with a step size of $2.5\times10^{-4}\,a_0$. Data needed for subsequent calculations (e.g., potential, normal mode frequencies, etc.) were stored at intervals of $2.5\times10^{-3}\,a_0$ along the path. Unlike the model system used previously,[27] the potential energy surface used

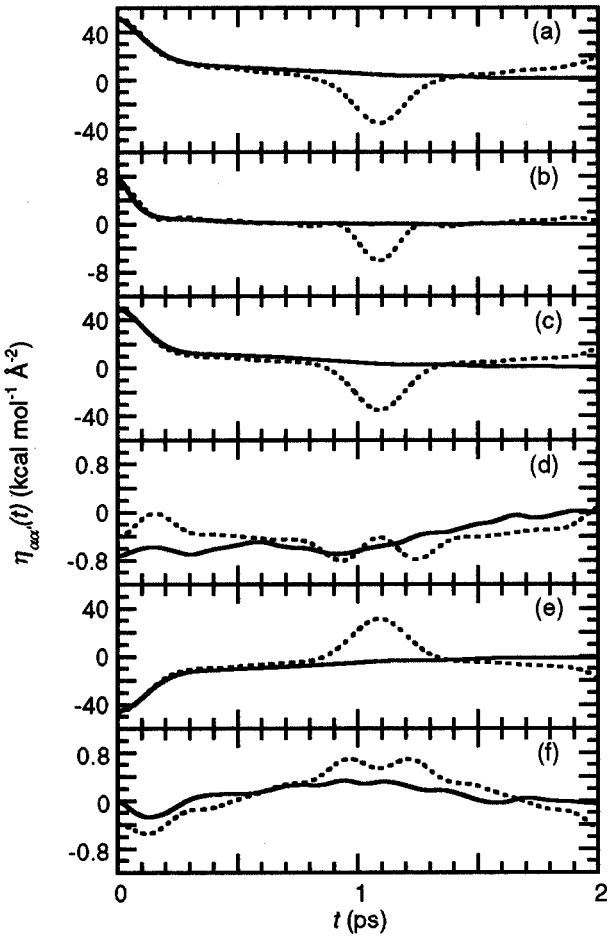

FIG. 4. Elements of the friction tensor in the **z** coordinate system as a function of time t: (a) η_{AA}, (b) η_{BB}, (c) η_{HH}, (d) η_{AB}, (e) η_{AH}, (f) η_{BH}. Solid curves are the results of molecular dynamics simulations of the force–force correlation functions, and dashed curves are the fits of the friction tensors to the cosine expansion in Eq. (61). Note that the scale of part (b) is a factor of 5 smaller than that for parts (a), (c), and (e), and that the scale of parts (d) and (f) is a factor of 10 smaller than that for part (b).

here has a minimum in each of the reactant and product channels. As the reaction path approaches either of these wells, the magnitude of the gradient gets smaller, leading to instability in the Euler integration method. To avoid this, an arbitrarily chosen cutoff in the magnitude of the gradient is used to switch from an Euler integration method to a multidimensional Newton–Raphson search for the location of the nearby well minimum. The MEP is then connected to the well bottom. Normal modes and harmonic frequencies were calculated in directions orthogonal to the MEP at each storage interval along the MEP.

The potential, frequencies, and CMS-0 potential along the MEP are shown in Fig. 5 as a function of the reaction coordinate s. The CMS-0 potential for the ES model is defined by Eq. (35), and that for the NES model is defined by the same equation, except that V_{ESP} is replaced by V_{NESP} and the coupled vibrational frequencies along the NESP are used instead of the uncoupled ones along the ESP. Note that the CMS-0 potential is the effective potential for tunneling in liquid-phase reactions,[10] and it is generalization of the vibrationally adiabatic ground-state potential[20,54] that is used for gas-phase reactions. Although the frequencies along the ESP and NESP are generally different, in this case we see that they are approximately equal, indicating small coupling between the solute and solvent. In addition to the real frequencies shown in Fig. 5, it is interesting to note the imaginary frequencies at the saddle point. These are 2248i cm^{-1} for the ES model and 2246i cm^{-1} for the NES model. Replacing the proton by a deuteron changes these values to 1597i and 1594i cm^{-1}, respectively. These are rather large imaginary frequencies, which indicates a narrow barrier.

V. RESULTS AND DISCUSSION

Computed rate constants for transfer of a proton and deuteron are reported in Table IV. In addition to the VTST/MT results, we present calculations from approximate TST approaches that treat the two dimensions in the equilibrium solvation model at different levels of theory: harmonic versus anharmonic and classical versus quantum mechanical. These latter calculations allow us to assess the importance of anharmonicity and the validity of a mixed quantum-classical treatment. Expressions for k_{CACA}^{TST}, k_{CACH}^{TST}, k_{CHCH}^{TST}, k_{CAQH}^{TST}, k_{CHQH}^{TST}, k_{QHQH}^{TST}, $k_{CAQH}^{TST/PT}$, $k_{CHQH}^{TST/PT}$, $k_{QHQH}^{TST/PT}$, $k_{CAQH}^{TST/UST}$, $k_{CHQH}^{TST/UST}$, and $k_{QHQH}^{TST/UST}$ are presented in Appendix B. The notation $k_{wxyz}^{TST/t}$ indicates the treatment of the R coordinate (wx) and r coordinate (yz) and tunneling correction factor (t). Subscripts w and y can be C or Q to indicate classical or quantum treatment, and x and z can be A or H to indicate an anharmonic or harmonic treatment. The superscript t can be blank to indicate no tunneling contribution, PT to indicate tunneling is approximated through 1-D barriers for each R using a parabolic approximation to the barrier, or UST to indicate that tunneling is treated by a uniform semiclassical tunneling approximation based on a 1-D cut through $W(r,R)$. The first 12 rows in Table IV are the results of these TST approximations as defined in Appendix B. The next three rows are results of the semiclassical VTST and VTST/MT calculations for the equilibrium solvation (ES) model, and the final three rows are results of the semiclassical VTST and VTST/MT calculations for the nonequilibrium solvation (NES) model. The bottom row is our most complete calculations, and all the other rows show the effects of various further approximations.

Comparison of the rate constants in the first 12 rows of Table IV allows us to assess the importance of quantization and anharmonicity on the computed rate constants. The purely classical rate constants (rows 1–3) all agree to within a few percent indicating that a harmonic treatment of the classical rate constant is adequate. Rows 4 and 5 show that quantization of the r degree of freedom (corresponding to the light H-atom motion) increases the rate constant by a factor of 200, whereas comparisons of rows 5 and 6 show that quantization of the R degree of freedom (corresponding to the heavier AB relative motion) has a much smaller effect on the rate constant. The reasonably good agreement between the mixed classical-quantum rate constant, k_{CAQH}^{TST}, and the quantum harmonic one, k_{QHQH}^{TST}, validates (within 35%–40%) the mixed treatment of the rate constant when tunneling is excluded. For the system studied here the quantum harmonic rate constant k_{QHQH}^{TST} is essentially equivalent to the conven-

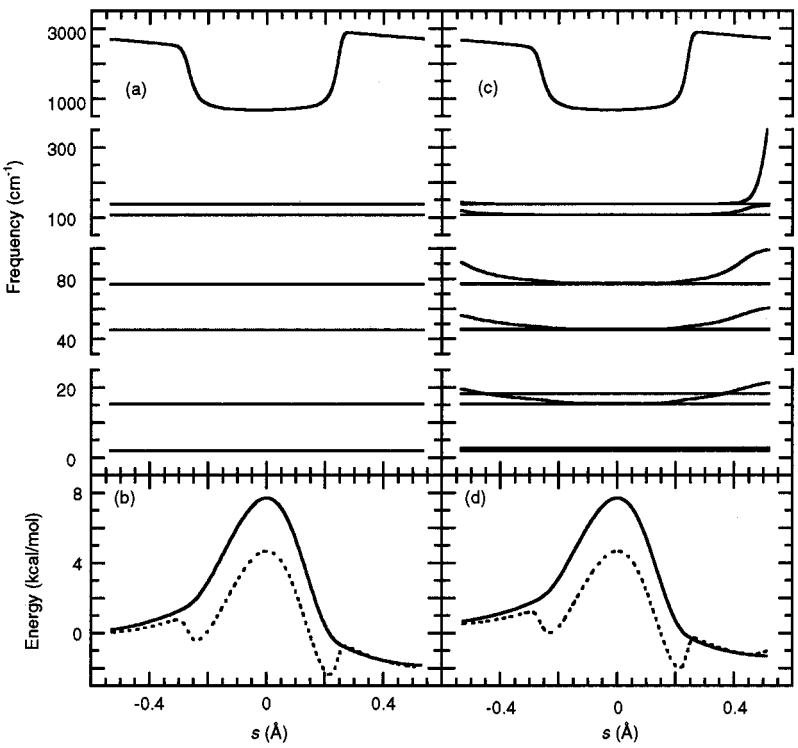

FIG. 5. Frequencies and energies as a function of distance s along the minimum energy path. Parts (a) and (b) are for the reaction with no coupling to the solvent friction (equilibrium solvation), and parts (c) and (d) are for the reaction with friction (nonequilibrium solvation). The frequencies displayed in parts (a) and (c) are for the normal modes orthogonal to the minimum energy path. The top most frequency is for the mode that corresponds to AB vibration in the solute. The lower frequencies are six sets of three frequencies, as discussed below Eq. (63), which are degenerate in the equilibrium solvation model. The solid and dashed curves in parts (b) and (d) are for the potential of mean force $W(r,R)$ and CMS-0 potential, respectively. The zero of energy for these curves is taken to be the energy at the reactant minimum.

tional quantized harmonic TST expression (see Appendix B), and comparison of rows 6 and 13 shows it agrees quite well with the quantized CVT rate constant for the equilibrium solvation model, $k_{\mathrm{ES}}^{\mathrm{CVT}}$.

Next consider the inclusion of tunneling. Tunneling of the light H-atom is quite important for this system, and in fact the parabolic tunneling result, $k_{\mathrm{CAQH}}^{\mathrm{TST/PT}}$, in row 7 is 80 times larger than the rate constant neglecting tunneling, $k_{\mathrm{CAQH}}^{\mathrm{TST}}$ in row 4. The rate constant $k_{\mathrm{CAQH}}^{\mathrm{TST/PT}}$ in Eq. (A23) is the closest expression to the "corrected" TST expression of Azzouz and Borgis.[7] The large difference in computed rate constants, 7.7×10^{7} for Azzouz and Borgis compared to 1.2×10^{11} computed here (row 7), is a consequence of different expressions for the probability densities $g(R)$. The close

TABLE IV. Approximate transition state theory and semiclassical VTST rate constants k_b^a (units of $10^{10}\,\mathrm{s}^{-1}$) and H/D kinetic isotope effect (H/D) for the proton and deuteron transfer reactions in the equilibrium and nonequilibrium solvation approximations.[a] $T=249$ K.

Row	a	b	H	D	H/D KIE
1	TST	CACA	7.5×10^{-4}	5.3×10^{-4}	1.4×10^{-4}
2	TST	CACH	7.6×10^{-4}	5.4×10^{-4}	1.4×10^{-4}
3	TST	CHCH	7.8×10^{-4}	5.5×10^{-4}	1.4×10^{-4}
4	TST	CAQH	0.15	0.015	10.
5	TST	CHQH	0.16	0.015	10.
6	TST	QHQH	0.11	0.010	10.
7	TST/PT	CAQH	12	0.10	120
8	TST/PT	CHQH	7.6	0.096	80.
9	TST/PT	QHQH	5.1	0.064	80.
10	TST/UST	CAQH	240	1.8	130
11	TST/UST	CHQH	82	1.1	74
12	TST/UST	QHQH	55	0.74	74
13	CVT	ES	0.11	0.010	10.
14[b]	CVT/ZCT	ES	11	0.53	21
15[b]	CVT/SCT	ES	16	1.0	16
16	CVT	NES	0.10	0.010	10.
17[b]	CVT/ZCT	NES	8.3	0.41	20.
18[b]	CVT/SCT	NES	13	0.85	15

[a]The first 12 rows are TST results for equilibrium solvation (ES) and use the notation $k_{wxyz}^{\mathrm{TST}/t}$ explained in the first paragraph of Sec. V. The last six rows are CVT and CVT/t results in the equilibrium solvation and nonequilibrium solvation approximations and have $wxyz=$QHQH, with t being ZCT or SCT.
[b]VTST/MT calculations.

agreement of our results for the mixed classical-quantum rate constant k_{CAQH}^{TST} with the quantized CVT results (i.e., k_{ES}^{CVT}) provides evidence that we have used a consistent probability density in the mixed expression, Eq. (A23), since the same probability density is appropriate for both k_{CAQH}^{TST} and $k_{CAQH}^{TST/PT}$. Next we consider the effect of going beyond the parabolic approximation but retaining a one-dimensional model of tunneling; this yields $k_{CAQH}^{TST/UST}$ in row 10, which is based on a semiclassical procedure employing the conservation-of-vibrational-energy (see Appendix B) approximation. This method greatly enhances the tunneling and gives a rate constant about a factor of 20 larger than $k_{CAQH}^{TST/PT}$; this result illustrates the danger of parabolic approximations.

Comparing k_{CAQH}^{TST} (row 4) and k_{CHQH}^{TST} (row 5) shows that making the harmonic approximation on the R motion when the R coordinate is treated classically and r is quantized but tunneling is neglected has little effect on the computed rate constant. However, the effects are larger when tunneling is included. For example, compare $k_{CAQH}^{TST/PT}$ with $k_{CHQH}^{TST/PT}$ (row 7 vs row 8) or $k_{CAQH}^{TST/UST}$ with $k_{CHQH}^{TST/UST}$ (row 10 vs row 11). The CAQH method averages the tunneling correction factors over R and the shape of the effective potential in r changes for different values of R. The narrower potentials in r at larger R values enhance the tunneling over the value of the tunneling factor at the saddle point. In the CHQH methods the effective quadratic potential results in the effective r potential being the same for all R values and equal to its value at the saddle point.

Next we compare the approximate QHQH methods with tunneling to the CVT/MT results for the equilibrium solvation model. The CVT/MT method includes multidimensional tunneling effects in that they are based on the zero-order canonical mean shape approximation and the SCT method includes a further multidimensional effect, namely corner-cutting tunneling, because it employs the small-curvature approximation to the effective mass. The best approximation to the equilibrium solvation rate constant is given by $k_{ES}^{CVT/SCT}$ (row 15), which includes the effect of reaction-path curvature on the tunneling; in particular, multidimensional tunneling is treated by the small-curvature tunneling approximation by using Eq. (36). Comparison with the rate constant that neglects reaction-path curvature, $k_{ES}^{CVT/ZCT}$ (row 14), indicates that the multidimensional ''corner-cutting'' effect enhances the rate constant by about 50%. The CVT/SCT results for the equilibrium solvation model are about 33% higher than the $k_{CAQH}^{TST/PT}$ results and a factor of 15 smaller than the $k_{CAQH}^{TST/UST}$ results. The better agreement with $k_{CAQH}^{TST/PT}$ for the H isotope is fortuitous since $k_{CAQH}^{TST/PT}$ neglects reaction-path curvature and tunnels through the bare potential of mean force, whereas the CVT/SCT results include the effects of reaction-path curvature and tunneling through the zero-order canonical mean-shape barrier. Furthermore, $k_{CAQH}^{TST/PT}$ and $k_{ES}^{CVT/SCT}$ differ by over a factor of 5 for the D isotope. Comparison of the multidimensional VTST results and those from ''corrected'' TST based on one-dimensional cuts for fixed R show that the latter approach is not adequate for treating the dynamics of this type of reaction for which tunneling is important.

The large-curvature ground-state tunneling (LCT) method[57,63] is often the most appropriate tunneling method for systems that display large reaction-path curvature such as a light-atom transfer reaction between two heavy moieties, which is studied here. In this method, the tunneling path for a given tunneling energy is taken to be a straight-line path between turning points along the MEP of the CMS-0 potential. For reactions with large reaction-path curvature, these paths may exhibit much greater corner cutting than the implicit paths of the SCT approximation and thus greatly reduce the tunneling distance, and thereby enhance tunneling. In the present case, the region of the potential where tunneling is important does not have large reaction-path curvature, even though the system does exhibit large curvature for some parts of the MEP. Reaction-path curvature is defined by $\kappa(s)=|\partial^2\mathbf{x}/\partial s^2|$, where $\mathbf{x}(s)$ is the vector of mass-weighted coordinates along the MEP. For straight-line paths, $\kappa(s)$ is zero. First note in Fig. 3(a) that the minimum energy path is a nearly straight line that is parallel to the r axis from about $r=1.05$ to 1.55 Å. In Fig. 6 we have plotted $\kappa(s)$ for the proton transfer reaction in the equilibrium solvation model. The curvature is quite large near $s=\pm 0.2-0.3$ Å, which corresponds to values of r in Fig. 3(a) near the potential minima. The zero-order canonical mean shape potential for proton transfer is also plotted in Fig. 6, and its peak and most of the barrier in $V^{CMS\text{-}0}$ lies between the peaks in $\kappa(s)$. The horizontal line in Fig. 6 is the value of the energy for the zero-point motion in the reactant well, which is the lowest energy for which tunneling occurs. Although we have not performed LCT calculations in the present study, it would be interesting to do so.

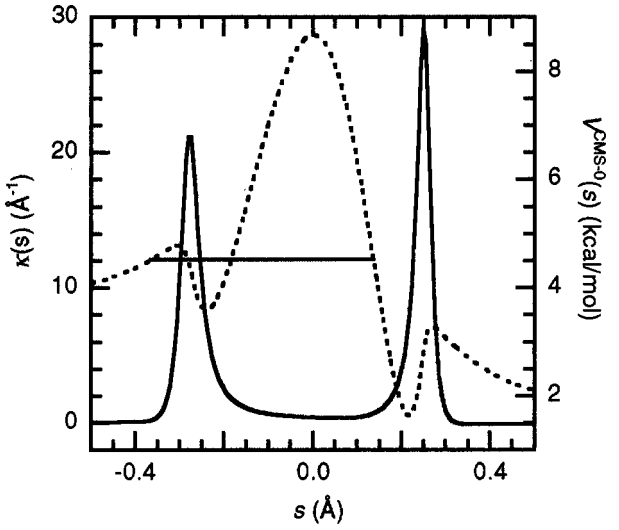

FIG. 6. Reaction path curvature $\kappa(s)$ (solid line) and CMS-0 potential (dashed line) as a function of distance s along the minimum energy path for the proton transfer reaction in the equilibrium solvation approximation. The horizontal line segment indicates the zero-point energy level in reactants, which is the lowest energy for which tunneling can occur.

Comparison of the rate constants calculated for the nonequilibrium solvation model with those for the equilibrium solvation model indicates that the effects of nonequilibrium solvation are small. In the classical limit the ratio of the nonequilibrium solvation and equilibrium solvation conventional TST rate constants is the classical Grote-Hynes factor.

For the friction model computed here, this factor is 0.99. The size of the Grote-Hynes factor is influenced by the magnitude and time scale of the friction and also by the size of the imaginary frequency at the saddle point. For the system studied here the largest components of the friction tensor, AA, HH, and AH in Fig. 4, can be fit to the Gaussian functional form

$$\eta(t) \approx \eta^{(1)}(0)\exp\left[-\frac{1}{2}\left(\frac{t}{\sigma^{(1)}}\right)^2\right] + \eta^{(2)}(0)\exp\left[-\frac{1}{2}\left(\frac{t}{\sigma^{(2)}}\right)^2\right], \quad (68)$$

where the time scales $\sigma^{(1)}$ and $\sigma^{(2)}$ are about 100 and 700 fs. The time scale for barrier crossing, which is determined by the imaginary frequency ω_b ($2248i$ cm^{-1} for H) at the saddle point, is about 2 fs and is therefore much faster than the frictional time scale. In a one-dimensional classical barrier-crossing model the Grote-Hynes correction factor is given by[50]

$$(\kappa^{\mathrm{GH}})^2 + \frac{\kappa^{\mathrm{GH}}}{\omega_b}\int_0^\infty dt\,\exp(-\kappa^{\mathrm{GH}}|\omega_b|t)\,\frac{\eta(t)}{\mu} - 1 = 0, \quad (69)$$

where μ is the effective mass for the one-dimensional motion. For a single Gaussian form for $\eta(t)$, values of $\sigma^{(1)} = 100$ fs and $\eta^{(1)} = 12$ kcal/mol Å^{-2} reproduce the Grote-Hynes factor in the multidimensional model. Using this model for the friction in Eq. (69), the exponential function in the integral damps out much more quickly than the friction, except for very small values of κ^{GH}. For the magnitude of the friction and imaginary frequency used in the model, κ^{GH} is close to unity. In this case, $\eta(t)$ is a weakly varying function of time over the time period for which the exponential in Eq. (69) damps out, and therefore the time scale of the friction is not an important factor in determining κ^{GH}. In fact, κ^{GH} is a monotonically decreasing function of the time scale σ, and the time scale is so large that further increase of $\sigma^{(1)}$ has negligible effect on κ^{GH}. We have computed sensitivities of κ^{GH} to changes in the barrier frequency, time scale, and magnitude of the friction for this model (e.g., $\partial \ln \kappa^{\mathrm{GH}}/\partial \ln \sigma^{(1)}$). The sensitivity of κ^{GH} to $\sigma^{(1)}$ is about -2×10^{-5}, while the sensitivities to ω_b and $\eta^{(1)}$ are 0.03 and -0.01, respectively. Thus, changing the time scale of the friction has little affect on κ^{GH}. On the other hand, the Grote-Hynes factor is decreased to a value below 0.6 when the barrier frequency is lowered by a factor of 5 (from $2228i$ cm^{-1} to $450i$ cm^{-1}). The effect of increasing the magnitude of the friction is less; increasing $\eta^{(1)}$ by a factor of 5 decreases κ^{GH} to only 0.92. The fact that a Grote-Hynes factor near one-half can be obtained by decreasing ω_b, but with no change to the friction, indicates that it is not a small magnitude of the friction that is responsible for the value of the Grote-Hynes factor being near unity. Instead, it is the large imaginary frequency that reduces the effect of nonequilibrium solvation in the classical rate constants. The effect of quantizing the bound degrees of freedom does not quantitatively change the effects of nonequilibrium solvation, as the ratio of the quantized CVT results $k_{\mathrm{NES}}^{\mathrm{CVT}}/k_{\mathrm{ES}}^{\mathrm{CVT}}$ is also 0.99. In our previous work we found that friction can have a larger effect on quantum mechanical tunneling.[24,26] This is also true in the present case, where the ratio $k_{\mathrm{NES}}^{\mathrm{CVT/SCT}}/k_{\mathrm{ES}}^{\mathrm{CVT/SCT}}$ is 0.81.

Our best estimate of the rate constant for this system is obtained by the CVT/SCT method for the nonequilibrium solvation model (row 18 of Table IV). The H/D kinetic isotope effect (KIE) from the semiclassical VTST and VTST/MT calculations ranges from 10 to 21, with our most complete calculation yielding 15. As noted above, tunneling contributes significantly to the rate constant for this light atom transfer reaction, and the tunneling correction factor is smaller for the heavier D atom; as a consequence the KIE increases from a value of 10 when tunneling is neglected to a value of 15 or more when it is included. The effect of reaction-path curvature (included in the SCT tunneling method but not the ZCT method) increases the rate constant for deuteron transfer more than for proton transfer (even though the SCT tunneling factor is still larger for the proton transfer), so that the KIE for the CVT/SCT method is about 15 while the KIE for the CVT/ZCT method is about 20. The KIEs obtained from the mixed classical-quantum methods including tunneling, i.e., $k_{\mathrm{CAQH}}^{\mathrm{TST/PT}}$ and $k_{\mathrm{CAQH}}^{\mathrm{TST/UST}}$ overestimate the kinetic isotope effect by factors of 8.0 and 8.7, respectively.

Table V compares rate constants computed previously by other methods[7–9,13,14] to those by the CVT/SCT method in the nonequilibrium solvation approximation. First note that the rate constants vary by over two orders of magnitude for the different methods. The systematic comparison of 18 combinations of approximations in Table IV, as discussed above, will help us to place these differences in perspective.

First consider the ''corrected'' classical TST results,[7] which are a factor of 1700 lower than the NES-CVT/SCT results. As discussed above, this appears to result from an incorrect treatment of the probability density $g(R)$ in Eq. (A5).

Next consider rows 2, 3, and 7 of Table V. The surface hopping (MDQT) results of Hammes-Schiffer and Tully[9] agree with our CVT/SCT results within 31% for H transfer, but this good agreement is most likely fortuitous because agreement is much worse (more than a factor of 4 deviation) for D. The curve-crossing TST[7] and path-integral TST[7,8] results differ even more from the NES-CVT/SCT curve results, in particular by factors ranging from 12 to 50. The curve-crossing TST, path-integral TST, and surface-hopping method all treat the proton quantum mechanically and the other coordinates classically. Our analysis above of mixed (CAQH) classical-quantum models of the rate constant for the equilibrium solvation model shows that this type of mixed approach (i.e., treating r quantum mechanically and R classically) is not appropriate for reactions in which tunneling is important. In particular, the mixed classical-quantum approach with tunneling included by a semiclassical approach for the actual potential of mean force (row 10 of Table IV) is over an order of magnitude larger than our more accurate CVT/SCT method, whereas introducing further approximations for the tunneling (as in rows 7–9 of Table IV) can convert this to an underestimate. Previous comparisons of VTST/MT and PI-QTST results for a model reaction in a liquid showed that they agreed well.[24] Thus the severe un-

TABLE V. Previously calculated rate constants ($10^{10}\,s^{-1}$) and KIEs compared to $k_{NES}^{CVT/SCT}$ from the present work for the proton and deuteron transfer reactions.

	H	D	H/D KIE
"Corrected" classical TST[a]	0.0077		
Curve-crossing TST[b]	0.78	0.017	46
PI-QTST[c]	1.1	0.026	40
QK (MFP)[d]	0.065		
QK (gas-phase V, linear coupling)[e]	0.99	0.012	83
QK (gas-phase V, nonlinear coupling)[f]	8.6	0.23	37
MDQT[g]	7.8	2.0	3.9
$k_{NES}^{CVT/SCT}$	13	0.85	15

[a]Average of one-dimensional TST rate constants for fixed R values (Azzouz and Borgis, Ref. 7).
[b]Landau–Zener curve-crossing TST method (Azzouz and Borgis, Ref. 7).
[c]Calculation by Azzouz and Borgis (Refs. 7 and 8) using the centroid path-integral quantum TST method of Voth and co-workers (Refs. 5 and 32).
[d]Quantum Kramers approach using effective "mean-field" potential and linear coupling to bath (Antoniou and Schwartz, Ref. 13).
[e]Quantum Kramers approach using gas-phase potential and linear coupling to bath (Antoniou and Schwartz, Ref. 13).
[f]Quantum Kramers approach using gas-phase potential and nonlinear coupling to bath (Antoniou and Schwartz, Ref. 14).
[g]Trajectory surface hopping approach (molecular dynamics with quantum transitions, Hammes-Schiffer and Tully, Ref. 9).

derestimate afforded by PI-QTST in Table V is surprising.

The surface hopping approach agrees better with the CVT/SCT method, and the results may be understood in part from the results in Table IV. Table IV show that $k_{CAQH}^{TST}/k_{QHQH}^{TST}$ is 1.4 for H and 1.5 for D. Thus we expect that if the *only* approximation is to use classical mechanics for the heavy-particle solute coordinate, one might see a deviation from a QHQH result like the NES-CVT/SCT one of about this magnitude. Table V show that $k_{MDQT}/k_{NES}^{CVT/SCT}$ is 0.6 for H and 2.4 for D, within about a factor of 2 of the expected deviation. This comparison is complicated by the lack of an explicit reactant partition function in the surface hopping approach. The source of the disagreement might, however, be due to tentative quantum transitions in the surface hopping method that are "frustrated" (and therefore do not occur) because the surface hops that are required for self-consistency in this method are sometimes forbidden by the conservation of total energy or the requirement that the momentum change be in the nonadiabatic coupling direction.[64]

The quantum Kramers approach[13,14] (rows 4–6 of Table IV) treats all coordinates in an effective GLE Hamiltonian on an equal footing and in this regard is similar to our approach. However, the GLE Hamiltonian used by Antoniou and Schwartz is different than the one we use. Our Hamiltonian includes three coordinates for the solute system plus bath modes representing the solvent friction. The potential in the absence of friction is the potential of mean force, which we calculate explicitly from molecular dynamics simulations. Antoniou and Schwartz treat the solute system as a single reaction coordinate that is coupled to bath modes representing the solvent friction. They have used two different functions for the potential in the absence of friction: the bare gas-phase potential and the gas-phase potential plus the diagonal terms arising from the friction [e.g., the terms that go like $(C_{j\alpha}z_\alpha)^2$ in Eq. (22)]. Their computed rate constants using the bare gas-phase potential agree better with the results of Azzouz and Borgis, when the coupling between the solute and bath is linear. Interestingly, they find that replacing the linear coupling with nonlinear coupling significantly changes the rate constant. This is contrary to our finding that solvent friction has a small effect on the computed rate constant.

The H/D kinetic isotope effects also show a large variation with the different methods of calculation ranging from 3.9 to 83. The largest values of the KIEs (40–83) are reminiscent of the large KIEs seen in the "corrected" TST calculations in which tunneling is inconsistently applied (e.g., rows 7–12 of Table IV). The relatively low value of the KIE predict by the MDQT method, 3.9, is the lowest and it is inconsistent with the VTST calculations, even those without tunneling corrections, which predict a value of 10. Our best estimate of the KIE with the NES-CVT/SCT method is 15. Kinetic isotope effects this large are generally cited as an indication of quantum mechanical tunneling.[65] In our previous studies of gas-phase reactions with barriers comparable to the one in the current model and for light-atom transfer, we found that VTST/MT gives good estimates of accurate H/D KIEs.[22,66,67] For one system with a comparable mass combination and barrier height (collinear Cl+HCl) the accurate H/D KIE was only 8 at 250 K.[66]

VI. CONCLUSIONS

We have presented a systematic approach to applying semiclassical variational transition state theory with multidimensional tunneling (VTST/MT) to proton transfer reactions in polar solution, and we have illustrated the approach by applying it to a model system that is of especially high interest because it has been widely studied by previous workers. In the VTST/MT approach as implemented here, the effects of the solvent on the proton transfer reaction are included using a generalized Langevin equation (GLE). The potential of mean force and solvent friction, which enter into

the GLE, are obtained from molecular dynamics simulations of the explicit solvent molecules interacting with the reactive solute system. The GLE dynamics are approximated by an effective Hamiltonian, which includes explicit bath modes that are treated as harmonic oscillators coupled to the solute coordinates. Then the VTST/MT method, including quantization of bound vibrational modes and multidimensional semiclassical tunneling corrections, is applied to the effective GLE Hamiltonian.

Rate constants calculated with and without solvent friction and with and without inclusion of tunneling allow us to assess the importance of these effects. It is not surprising that quantum mechanical tunneling is important for this light-atom transfer reaction. The rate constants are enhanced by as much as two orders of magnitude by including tunneling effects. It is somewhat surprising that the effect of solvent friction is very small for this reaction that involves charge transfer in a polar solvent. An analysis of the effect of nonequilibrium solvation indicates that the narrowness (reflected in the large imaginary frequency, $2248i\ \mathrm{cm}^{-1}$ for H) of the potential barrier at the saddle point leads to poor coupling between the dynamics of the solvent bath and the proton transfer.

Previous calculations on the model problem studied here have exhibited a wide variation in the rate constants calculated by different theoretical approaches. Also, the previous methods have predicted an H/D kinetic isotope effect (KIE) that ranges from about 4 to 83. Our most reliable estimate of the H/D KIE is 15. The wide variation of computed rate constants and KIEs with different methods is an indication of the difficulty of accurately computing rate constants for reactions in condensed phases when quantum mechanical effects are important. Accurate benchmark calculations are more difficult to perform in this case, so we rely on comparisons of the results of approximate methods to gain insight into the reaction dynamics and applicability of different approximation to the system. By calculating the rate constant with a systematic sequence of approximations, we have clarified a number of the factors that help explain the differences between the various approximations in the literature. Nevertheless, there is opportunity for further studies to understand even better the sources of the differences between the calculated results for different methods.

ACKNOWLEDGMENTS

This work was supported by the Division of Chemical Sciences, Office of Basic Energy Sciences, of the U.S. Department of Energy. This research was performed in the William R. Wiley Environmental Molecular Sciences Laboratory a national scientific user facility sponsored by the Department of Energy's Office of Biological and Environmental Research and located at Pacific Northwest National Laboratory. Pacific Northwest National Laboratory is operated for the Department of Energy by Battelle. This work was also supported in part by the National Science Foundation. The authors wish to thank Sharon Hammes-Schiffer and John Tully for their participation in the early stages of the project and for helpful comments on the manuscript.

APPENDIX A: DERIVATION OF MEAN FORCE EXPRESSIONS [EQS. (45) AND (46)]

We define the rotational kinetic energy operator T_{rot} by

$$T_{\mathrm{rot}}=\frac{1}{2I(r,R)}\left(p_\theta^2+\frac{p_\phi^2}{\sin^2\theta}\right). \tag{A1}$$

Then the third term on the right hand side of the first line of Eq. (45) is just

$$\left\langle \frac{\partial}{\partial r}\left[\frac{1}{2I(r,R)}\left(P_\theta^2+\frac{P_\phi^2}{\sin^2\theta}\right)\right]\right\rangle_{r,R}=\left\langle \frac{\partial}{\partial r}T_{\mathrm{rot}}\right\rangle_{r,R}. \tag{A2}$$

The only r and R dependence in T_{rot} is due to $I(r,R)$, so that the derivative of T_{rot} with respect to r can be rewritten

$$\frac{\partial}{\partial r}T_{\mathrm{rot}}=\left(p_\theta^2+\frac{p_\phi^2}{\sin^2\theta}\right)\left(\frac{\partial}{\partial r}\left[\frac{1}{2I(r,R)}\right]\right)=\left(-\frac{\partial \ln I}{\partial r}\right)T_{\mathrm{rot}}. \tag{A3}$$

Substituting Eq. (A3) into (A2) we obtain

$$\begin{aligned}\left\langle \frac{\partial}{\partial r}\left[\frac{1}{2I(r,R)}\left(P_\theta^2+\frac{P_\phi^2}{\sin^2\theta}\right)\right]\right\rangle_{r,R}&=-\frac{\partial \ln I}{\partial r}\langle T_{\mathrm{rot}}\rangle_{r,R}\\&=-k_{\mathrm{B}}T\frac{\partial \ln I}{\partial r},\end{aligned} \tag{A4}$$

where $\partial \ln I/\partial r$ is just a constant in the averages in Eq. (A2) since $I(r,R)$ depends only on the coordinates r and R and not on any other coordinates in the system. We have used the equipartition of energy to give $\langle T_{\mathrm{rot}}\rangle=-k_{\mathrm{B}}T$ in this expression. Similar arguments can be made to evaluate the third term on the right hand side of the first line of Eq. (46):

$$\begin{aligned}\left\langle \frac{\partial}{\partial R}\left[\frac{1}{2I(r,R)}\left(P_\theta^2+\frac{P_\phi^2}{\sin^2\theta}\right)\right]\right\rangle_{r,R}&=-\frac{\partial \ln I}{\partial R}\langle T_{\mathrm{rot}}\rangle_{r,R}\\&=-k_{\mathrm{B}}T\frac{\partial \ln I}{\partial R}.\end{aligned} \tag{A5}$$

APPENDIX B: APPROXIMATE TWO-DIMENSIONAL TRANSITION-STATE THEORY APPROACHES

In the equilibrium solvation approximation the classical TST rate constant k_C^{TST} is given by[68]

$$\begin{aligned}Q_{\mathrm{C}}^R(T)k_{\mathrm{C}}^{\mathrm{TST}}(T)=\frac{1}{(2\pi\hbar)^2}\int dP_R\int dP_r\int dR\int dr\\ \times\exp(-H_{\mathrm{ES}}/k_{\mathrm{B}}T)\,\delta(Z)\dot{Z}\,\theta(\dot{Z}),\end{aligned} \tag{B1}$$

where the equilibrium solvation Hamiltonian is given by

$$H_{\mathrm{ES}}=\frac{1}{2}(P_r,P_R)\boldsymbol{\mu}^{-1}\begin{pmatrix}P_r\\P_R\end{pmatrix}+W(r,R) \tag{B2}$$

in which $\delta(x)$ is the Dirac delta function, $\theta(x)$ is the Heaviside function, Z is a function of coordinates r and R such that

$Z(r,R)=0$ defines the transition-state dividing surface, and $Q_C^R(T)$ is the classical reactant partition function, which is discussed below. We choose the dividing surface by

$$Z(r,R)=r-r_b(R) \tag{B3}$$

and $r_b(R)$ is the location of the maximum in $W(r,R)$ for fixed value of R. Note that the choice of dividing surface in Eq. (B3) is different than that assumed in conventional TST. In conventional TST the dividing surface is chosen to be perpendicular to the minimum-energy isoinertial reaction path at the saddle point, and for the two-dimensional system studied here, the conventional dividing surface corresponds to the bound normal mode coordinate at the saddle point. The normal mode will depend on the masses of the system, whereas the definition in Eq. (B3) does not depend upon the masses, so they will not be the same in general. However, the normal modes at the saddle point are almost pure r and R motion for the system studied here, so for the present example, TST based on the conventional dividing surface and TST based on Eq. (B3) agree to within a couple of percent for all cases where we compared them.

For the choice of dividing surface in Eq. (B3), the expression for $k_C^{\mathrm{TST}}(T)$ in Eq. (B1) can be reduced to a one-dimensional integral over R

$$k_C^{\mathrm{TST}}(T)=\int dR g(R) k_C^{\mathrm{TST,1D}}(R,T). \tag{B4}$$

The classical one-dimensional TST rate constant for a fixed value of R is given by

$$k_C^{\mathrm{TST,1D}}(R,T)=\frac{k_B T}{hQ^r(R,T)}\exp[-W_b(R)/k_B T], \tag{B5}$$

where the function $Q^r(R,T)$ is the reactant partition function in the one-dimensional potential (as a function of r) at fixed R,

$$W_b(R)=W[r_b(R),R] \tag{B6}$$

is the value of the potential of mean force at its local maximum for fixed R, and the equilibrium probability density in R is defined by

$$g(R)=\frac{Q^r(R,T)}{hQ_C^{\mathrm{R}}(T)}[2\pi k_B T \det(\boldsymbol{\mu})]^{1/2} \times\left|\boldsymbol{\mu}^{-1/2}\cdot\begin{pmatrix}1\\ -dr_b/dR\end{pmatrix}\right|. \tag{B7}$$

Expression of the TST rate constant as an integral of one-dimensional rate constants as expressed in Eq. (B4) is similar to the ''corrected'' classical theory presented by Azzouz and Borgis.[7] In the previous work the weighting factor was defined as the ''probability distribution function for R in the reactant region, $r<r_b(R)$,'' but no explicit expression was provided. The ratio $Q^r(R,T)/Q_C^{\mathrm{R}}(T)$ in our expression for the probability density is the probability density in R in the reactant region. The remaining terms in Eq. (B7) result from the integration over the momentum integrals in Eq. (B1) and combined with the ratio $Q^r(R,T)/Q_C^{\mathrm{R}}(T)$ give the correct weighting of the one-dimensional rate constants for each R in the classical TST expression.

Azzouz and Borgis modify the one-dimensional classical TST rate constant to account for quantization of the bound vibration in the r coordinates for reactants and to include tunneling through the one-dimensional barriers. This leads to a mixed quantum-classical expression in which the r degree of freedom is treated quantum mechanically while R is treated by a classical average. This previous approach is one motivation for us to examine the effects of quantization on the computed rate constants and the validity of mixed quantum-classical expressions for the rate constants. In addition, we wish to examine the importance of anharmonicity, which we can study explicitly in the classical calculations. The remainder of this appendix presents different approximate TST rate constants based upon the TST expression in Eq. (B4).

A consistent treatment of quantum mechanical effects in the TST rate constant requires including effects of quantization in the probability density $g(R)$ as well as the one-dimensional rates constants. For consistency, if effects of quantization are included in $g(R)$, they should also be included in the reactant partition function. The classical reactant partition function for the dividing surface in Eq. (B3) is given by

$$\begin{aligned}Q_C^{\mathrm{R}}(T)&=\frac{1}{(2\pi\hbar)^2}\int dP_R\int dP_r\int dR\int dr \\ &\quad\times\exp(-H_{\mathrm{ES}}/k_B T)\,\theta(-Z) \\ &=Q_{\mathrm{CACA}}^{\mathrm{R}}=\frac{k_B T(\det\boldsymbol{\mu})^{1/2}}{2\pi\hbar^2}\int dR\int dr \\ &\quad\times\exp[-W(r,R)/k_B T]\,\theta[r_b(R)-r],\end{aligned} \tag{B8}$$

where we have introduced the notation $Q_{\mathrm{CACA}}^{\mathrm{R}}$ to denote that both the r and R coordinates are being treated classically (C) and anharmonically (A). If the r potential for each fixed R is treated as a harmonic oscillator we approximate $Q_{\mathrm{CACA}}^{\mathrm{R}}$ by

$$\begin{aligned}Q_{\mathrm{CACH}}^{\mathrm{R}}(T)&=\left[\frac{k_B T m_B(m_A+m_H)}{2\pi\hbar^2 M}\right]^{1/2}\int dR \\ &\quad\times\exp[-W_0(R)/k_B T]Q_{\mathrm{CH}}^r(R,T),\end{aligned} \tag{B9}$$

where $W_0(R)\equiv W[r_0(R),R]$, $r_0(R)$ is the reactant minimum in $W(r,R)$ for fixed value of R, the reactant R-dependent frequency is defined by

$$\omega_r(R)=\left[\frac{1}{\mu_{\mathrm{AH}}}\frac{\partial^2 W(r,R)}{\partial r^2}\bigg|_{r=r_0(R)}\right] \tag{B10}$$

with $\mu_{\mathrm{AH}}=m_A m_H/(m_A+m_H)$, and

$$Q_{\mathrm{CH}}^r(R,T)=\frac{k_B T}{\hbar\omega_r(R)}. \tag{B11}$$

Replacing the classical partition given by Eq. (B11) by the quantized one in Eq. (B9) results in

$$\begin{aligned}Q_{\mathrm{CAQH}}^{\mathrm{R}}(T)&=\left[\frac{k_B T m_B(m_A+m_H)}{2\pi\hbar^2 M}\right]^{1/2}\int dR \\ &\quad\times\exp[-W_0(R)/k_B T]Q_{\mathrm{QH}(R,T)}^r,\end{aligned} \tag{B12}$$

where

$$Q^{r}_{\mathrm{QH}}(R,T)=\frac{1}{2\sinh[\hbar\omega_r(R)/2k_{\mathrm{B}}T]}. \tag{B13}$$

Treating both the r and R degrees of freedom as harmonic oscillators, the classical partition function is approximated by

$$Q^{\mathrm{R}}_{\mathrm{CHCH}}(T)=\frac{k_{\mathrm{B}}T}{\hbar\omega^{\mathrm{R}}_1}\frac{k_{\mathrm{B}}T}{\hbar\omega^{\mathrm{R}}_2}, \tag{B14}$$

where ω^{R}_1 and ω^{R}_2 are the harmonic frequencies of the reactant well; mode 1 is of low frequency and consists largely of R motion, and mode 2 is of high frequency and consists largely of r motion. The mixed classical-quantum and quantum partition functions in the harmonic approximation are given by

$$Q^{\mathrm{R}}_{\mathrm{CHQH}}(T)=\frac{k_{\mathrm{B}}T}{\hbar\omega^{\mathrm{R}}_1}\frac{1}{2\sinh(\hbar\omega^{\mathrm{R}}_2/2k_{\mathrm{B}}T)} \tag{B15}$$

and

$$Q^{\mathrm{R}}_{\mathrm{QHQH}}(T)=\frac{1}{2\sinh(\hbar\omega^{\mathrm{R}}_1/2k_{\mathrm{B}}T)}\frac{1}{2\sinh(\hbar\omega^{\mathrm{R}}_2/2k_{\mathrm{B}}T)}, \tag{B16}$$

The different approximations to the reactant partition function are used in Eq. (B7) along with the appropriate expression for $Q^r(R,T)$ to define the appropriate probability density. Since $Q^r(R,T)$ cancels out in the product of $g(R)$ and $k_{\mathrm{C}}^{\mathrm{TST,1D}}(R,T)$, its definition does not change the value of $k_{\mathrm{C}}^{\mathrm{TST}}(T)$, so we do not specify the explicit expression for $Q^r(R,T)$.

We now define approximate TST rate constants that are consistent with the definitions of the reactant partition function given in Eqs. (B8), (B9), (B14), (B15), and (B16). A purely classical expression is given by

$$k^{\mathrm{TST}}_{\mathrm{C}x\mathrm{C}z}(T)=\int dR g_{\mathrm{C}x\mathrm{C}z}(R)k_{\mathrm{C}}^{\mathrm{TST,1D}}(R,T), \tag{B17}$$

where x and z may be H or A, and $g_{\mathrm{C}x\mathrm{C}z}(R)$ indicates that $Q^{R}_{\mathrm{C}x\mathrm{C}z}$ is used for the reactant partition function in Eq. (B7). Mixed quantum-classical expressions, $k^{\mathrm{TST}}_{\mathrm{CAQH}}(T)$ and $k^{\mathrm{TST}}_{\mathrm{CHQH}}(T)$, excluding tunneling, are given by similar expressions, but with $g_{\mathrm{C}x\mathrm{C}z}(R)$ is replaced by $g_{\mathrm{CAQH}}(R)$ and $g_{\mathrm{CHQH}}(R)$, respectively. If the potential is treated harmonically about the saddle point and reactant, the classical rate constant reduces to

$$k^{\mathrm{TST}}_{\mathrm{CHCH}}(T)=\frac{k_{\mathrm{B}}T}{hQ^{\mathrm{R}}_{\mathrm{CHCH}}(T)}\frac{k_{\mathrm{B}}T}{\hbar\omega^{\ddagger}_R}\exp(-W^{\ddagger}/k_{\mathrm{B}}T), \tag{B18}$$

where $W^{\ddagger}$ is the value of the potential of mean force at the saddle point, and the frequency in R is given by

$$\omega^{\ddagger}_R=\left[\left(\frac{\partial^2W}{\partial r^2}\frac{\partial^2W}{\partial R^2}-\frac{\partial^2W}{\partial r\,\partial R}\frac{\partial^2W}{\partial r\,\partial R}\right)\times\left(\det(\boldsymbol{\mu})\left|\mu^{-1/2}\cdot\begin{pmatrix}\frac{\partial^2W}{\partial r^2}\\ \frac{\partial^2W}{\partial r\,\partial R}\end{pmatrix}\right|\right)^{-1}\right]_{r=r^{\ddagger},R=R^{\ddagger}}. \tag{B19}$$

Although this expression is not equivalent to the bound normal mode frequency at the saddle point, it is closely approximated by the normal mode frequency for the system studied here. The mixed classical-quantum harmonic expression, $k^{\mathrm{TST}}_{\mathrm{CHQH}}(T)$, is obtained by replacing $Q^{\mathrm{R}}_{\mathrm{CHCH}}$ by $Q^{\mathrm{R}}_{\mathrm{CHQH}}$. The quantum harmonic expression, $k^{\mathrm{TST}}_{\mathrm{QHQH}}(T)$, is obtained by replacing $Q^{\mathrm{R}}_{\mathrm{CHCH}}$ by $Q^{\mathrm{R}}_{\mathrm{QHQH}}$ and by replacing the classical partition function for R at the saddle point by its quantum harmonic analogue to give

$$k^{\mathrm{TST}}_{\mathrm{QHQH}}(T)=\frac{k_{\mathrm{B}}T}{hQ^{\mathrm{R}}_{\mathrm{QHQH}}(T)}\frac{1}{2\sinh(\hbar\omega^{\ddagger}_R/2k_{\mathrm{B}}T)}\times\exp(-W^{\ddagger}/k_{\mathrm{B}}t). \tag{B20}$$

Tunneling is important for this light-atom transfer reaction and we consider including tunneling contributions in the mixed classical-quantum rate expression in a manner similar to that used by Azzouz and Borgis.[7] In their approach an effective parabolic barrier is fitted to the barrier height and width for each value of R and the parabolic tunneling probabilities are integrated to obtain the parabolic tunneling (PT) transmission coefficient:

$$\kappa^{\mathrm{PT}}(R,T)=\frac{\int_{W_0(R)}^{\infty}dE\exp(-E/kT)P^{\mathrm{PT}}(R,E)}{\int_{W_b(R)}^{\infty}dE\exp(-E/kT)}. \tag{B21}$$

In this expression $P^{\mathrm{PT}}(R,E)$ is the probability for tunneling through the parabolic barrier[37] in r for fixed R at energy E. The mixed classical-quantum expression, $k^{\mathrm{TST/PT}}_{\mathrm{CAQH}}(T)$, based on the parabolic approximation for tunneling contributions, is given by

$$k^{\mathrm{TST/PT}}_{\mathrm{CAQH}}(T)=\int dR g_{\mathrm{CAQH}}(R)\kappa^{\mathrm{PT}}(R,T)k_{\mathrm{C}}^{\mathrm{TST,1D}}(R,T). \tag{B22}$$

To assess the sensitivity of the calculated tunneling contributions to approximations that affect the barrier shape, we also compute the tunneling probabilities by a uniform semiclassical tunneling (UST) expression on the actual potential of mean force along the reaction path. Note that this UST approach and the PT approximation to it are based on the potential of mean force rather than the canonical mean shape[10] potential; thus these approximations are liquid-phase analogs of the conservation-of-vibrational-energy (CVE) approach[21] rather than the more physical vibrationally adiabatic[20,69] approach. As such, these approximations are true one-dimensional tunneling approximations, in contrast to the multidimensional ZCT, SCT, and LCT approaches that include the effects of vibrational energy in modes transverse

to the reaction coordinate. The uniform semiclassical approximation based on the one-dimensional potential of mean force yields $k_{\mathrm{CAQH}}^{\mathrm{TST/UST}}(T)$ where $\kappa^{\mathrm{PT}}(R,T)$ in Eq. (B22) is replaced by $\kappa^{\mathrm{UST}}(R,T)$, which is given by Eq. (B21) with $P^{\mathrm{PT}}(R,E)$ replaced by $P^{\mathrm{UST}}(R,E)$, and $P^{\mathrm{UST}}(R,E)$ is a uniform semiclassical tunneling probability[70] for the actual potential of mean force $W(r,R)$ as a function of r for fixed R. With the harmonic approximation for the R coordinate, Eq. (B22) reduces to

$$k_{\mathrm{CHQH}}^{\mathrm{TST/PT}}(T)=\kappa^{\mathrm{PT}}(R^{\ddagger},T)\,\frac{k_{\mathrm{B}}T}{hQ_{\mathrm{CHQH}}^{\mathrm{R}}(T)}\,\frac{k_{\mathrm{B}}T}{\hbar\omega_R^{\ddagger}}\times\exp(-W^{\ddagger}/k_{\mathrm{B}}T) \tag{B23}$$

and the quantum harmonic expression including tunneling, $k_{\mathrm{QHQH}}^{\mathrm{TST/PT}}(T)$, is given by Eq. (B20) multiplied by the parabolic correction factor $\kappa^{\mathrm{PT}}(R^{\ddagger},T)$ for tunneling through the 1-D potential in r for $R=R^{\ddagger}$, i.e., $W(r,R^{\ddagger})$. Analogous expressions for $k_{\mathrm{CHQH}}^{\mathrm{TST/UST}}(T)$ and $k_{\mathrm{QHQH}}^{\mathrm{TST/UST}}(T)$ are obtained by replacing $\kappa^{\mathrm{PT}}(R^{\ddagger},T)$ by $\kappa^{\mathrm{UST}}(R^{\ddagger},T)$.

[1] R. P. Bell, in *The Proton in Chemistry* (Chapman and Hall, London, 1973); *Proton Transfer Reactions*, edited by E. F. Caldin and V. Gold (Chapman and Hall, London, 1975); F. Hibbert, Adv. Phys. Org. Chem. **22**, 113 (1986); **26**, 255 (1990); *Electron and Ion Transfer in Condensed Media*, edited by A. A. Kornyshev, M. Tosi, and J. Ulstrup (World Scientific, Singapore, 1997).

[2] C. Walsh, *Enzymatic Reaction Mechanisms* (Freeman, San Francisco, 1979).

[3] M. R. Hoffman, in *Aquatic Chemical Kinetics*, edited by W. Stumm (Wiley-Interscience, New York, 1990), p. 71.

[4] R. A. Marcus, Faraday Symp. Chem. Soc. **10**, 60 (1975); A. Warshel, J. Phys. Chem. **86**, 2218 (1982); D. Borgis, S. Lee, and J. T. Hynes, Chem. Phys. Lett. **162**, 19 (1989); M. Morillo and R. I. Cukier, J. Chem. Phys. **92**, 4833 (1990); A. Warshel and Z. T. Chu, *ibid.* **93**, 4003 (1990); J. K. Hwang, Z. T. Chu, A. Yadav, and A. Warshel, J. Phys. Chem. **95**, 8445 (1991); A. Suárez and R. Silbey, J. Chem. Phys. **94**, 4809 (1991); D. Borgis, G. Tarjus, and H. Azzouz, J. Phys. Chem. **96**, 3188 (1992); D. Borgis, G. Tarjus, and H. Azzouz, J. Chem. Phys. **97**, 1390 (1992); D. Laria, G. Ciccotti, M. Ferriario, and R. Kapral, *ibid.* **97**, 378 (1992); H. J. C. Berendsen and J. Mavri, J. Phys. Chem. **97**, 13464 (1993); J.-K. Hwang and A. Warshel, *ibid.* **97**, 10053 (1993); J. Mavri, H. J. C. Berendsen, and W. F. van Gunsteren, *ibid.* **97**, 13469 (1993); P. Bala, B. Lesyng, and J. A. McCammon, Chem. Phys. **180**, 271 (1994); J. Lobaugh and G. A. Voth, J. Chem. Phys. **100**, 3039 (1994); K. Ando and J. T. Hynes, J. Mol. Liq. **64**, 25 (1995); R. Pomes and B. Roux, Chem. Phys. Lett. **234**, 416 (1995); A. Staib, D. Borgis, and J. T. Hynes, J. Chem. Phys. **102**, 2487 (1995); S. Hammes-Schiffer and J. C. Tully, J. Phys. Chem. **99**, 5793 (1995); D. Borgis and J. T. Hynes, *ibid.* **100**, 1118 (1996); J. Lobaugh and G. A. Voth, J. Chem. Phys. **104**, 2056 (1996); K. Ando and J. T. Hynes, J. Phys. Chem. B **101**, 10464 (1997); S. R. Billeter and W. F. van Gunsteren, Comput. Phys. Commun. **107**, 61 (1997); K. Ando and J. T. Hynes, J. Phys. Chem. A **103**, 10398 (1999); R. I. Cukier and J. Zhu, J. Chem. Phys. **110**, 9587 (1999).

[5] G. A. Voth, D. Chandler, and W. H. Miller, J. Chem. Phys. **91**, 7749 (1989); D. H. Li and G. A. Voth, J. Phys. Chem. **95**, 10425 (1991).

[6] D. Borgis and J. T. Hynes, J. Chem. Phys. **94**, 3619 (1991); D. Borgis and J. T. Hynes, Chem. Phys. **170**, 315 (1993).

[7] H. Azzouz and D. Borgis, J. Chem. Phys. **98**, 7361 (1993).

[8] H. Azzouz and D. Borgis, J. Mol. Liq. **61**, 17 (1994).

[9] S. Hammes-Schiffer and J. C. Tully, J. Chem. Phys. **101**, 4657 (1994).

[10] D. G. Truhlar, Y.-P. Liu, G. K. Schenter, and B. C. Garrett, J. Phys. Chem. **98**, 8396 (1994).

[11] H. Azzouz and D. Borgis, J. Mol. Liq. **63**, 89 (1995).

[12] D. Antoniou and S. D. Schwartz, J. Chem. Phys. **109**, 5487 (1998).

[13] D. Antoniou and S. D. Schwartz, J. Chem. Phys. **110**, 465 (1999).

[14] D. Antoniou and S. D. Schwartz, J. Chem. Phys. **110**, 7359 (1999).

[15] C. Alhambra, J. Gao, J. C. Corchado, J. Villà, and D. G. Truhlar, J. Am. Chem. Soc. **121**, 2253 (2000).

[16] H. Eyring, J. Chem. Phys. **3**, 107 (1935); H. Eyring, Trans. Faraday Soc. **34**, 41 (1938); S. Glasstone, K. J. Laidler, and H. Eyring, *The Theory of Rate Processes* (McGraw-Hill, New York, 1941); D. G. Truhlar, W. L. Hase, and J. T. Hynes, J. Phys. Chem. **87**, 2664 (1983).

[17] E. Wigner, J. Chem. Phys. **5**, 720 (1937).

[18] E. Wigner, Trans. Faraday Soc. **34**, 29 (1938).

[19] D. G. Truhlar, B. C. Garrett, and S. J. Klippenstein, J. Phys. Chem. **100**, 12771 (1996).

[20] D. G. Truhlar and B. C. Garrett, Acc. Chem. Res. **13**, 440 (1980); D. G. Truhlar, A. D. Isaacson, R. T. Skodje, and B. C. Garrett, J. Phys. Chem. **86**, 2252 (1982); D. G. Truhlar and B. C. Garrett, Annu. Rev. Phys. Chem. **35**, 159 (1984); D. G. Truhlar, A. D. Isaacson, and B. C. Garrett, in *Theory of Chemical Reaction Dynamics*, Vol. IV, edited by M. Baer (CRC, Boca Raton, FL, 1985), p. 65.

[21] B. C. Garrett and D. G. Truhlar, J. Phys. Chem. **83**, 1079 (1979).

[22] B. C. Garrett and D. G. Truhlar, J. Chem. Phys. **81**, 309 (1984); B. C. Garrett and D. G. Truhlar, J. Phys. Chem. **95**, 10374 (1991); T. C. Allison and D. G. Truhlar, in *Modern Methods for Multidimensional Dynamics Computations in Chemistry*, edited by D. L. Thompson (World Scientific, Singapore, 1998), p. 618.

[23] G. K. Schenter, R. P. McRae, and B. C. Garrett, J. Chem. Phys. **97**, 9116 (1992).

[24] R. P. McRae, G. K. Schenter, B. C. Garrett, G. R. Haynes, G. A. Voth, and G. C. Schatz, J. Chem. Phys. **97**, 7392 (1992); R. P. McRae and B. C. Garrett, *ibid.* **98**, 6929 (1993).

[25] B. C. Garrett and G. K. Schenter, Int. Rev. Phys. Chem. **13**, 263 (1994).

[26] B. C. Garrett and G. K. Schenter, in *Structure and Reactivity in Aqueous Solution*, Vol. 568, edited by C. J. Cramer and D. G. Truhlar (American Chemical Society, Washington, DC, 1994), p. 122; Y.-Y. Chuang, C. J. Cramer, and D. G. Truhlar, Int. J. Quantum Chem. **70**, 887 (1998); Y.-Y. Chuang and D. G. Truhlar, J. Am. Chem. Soc. **121**, 10157 (1999).

[27] R. P. McRae, G. K. Schenter, and B. C. Garrett, J. Chem. Soc., Faraday Trans. **93**, 997 (1997).

[28] C. Alhambra, J. Gao, J. C. Corchado, J. Villà, and D. G. Truhlar, J. Am. Chem. Soc. **122**, 8197 (2000).

[29] R. Zwanzig, in *Lectures in Theoretical Physics (Boulder)*, Vol. 3 (Wiley, New York, 1961), p. 135.

[30] R. Zwanzig, Annu. Rev. Phys. Chem. **16**, 67 (1965).

[31] H. Mori, Prog. Theor. Phys. **33**, 423 (1965); **34**, 399 (1965).

[32] G. A. Voth, J. Phys. Chem. **97**, 8365 (1993).

[33] J. C. Tully, J. Chem. Phys. **93**, 1061 (1990).

[34] S. D. Schwartz, J. Chem. Phys. **105**, 6871 (1996); **107**, 2424 (1997).

[35] W. H. Miller, S. D. Schwartz, and J. W. Tromp, J. Chem. Phys. **79**, 4889 (1983).

[36] T. Yamamoto, J. Chem. Phys. **33**, 281 (1960).

[37] R. P. Bell, Trans. Faraday Soc. **55**, 1 (1959).

[38] R. P. Bell, J. Chem. Soc., Faraday Trans. **76**, 954 (1980).

[39] R. Zwanzig, J. Stat. Phys. **9**, 215 (1973).

[40] B. Bigot, B. J. Costa-Cabral, and J. L. Rivail, J. Chem. Phys. **83**, 3083 (1985).

[41] W. L. Jorgensen, J. Phys. Chem. **87**, 5304 (1983).

[42] C. J. Cramer and D. G. Truhlar, Chem. Rev. **99**, 2161 (1999).

[43] D. Lim, C. Jenson, M. P. Repasky, and W. L. Jorgensen, in *Transition State Modeling for Catalysis*, edited by D. G. Truhlar (American Chemical Society Symposium Series Vol. 721, Washington, DC, 1999), p. 74.

[44] D. G. Truhlar, G. K. Schenter, and B. C. Garrett, J. Chem. Phys. **98**, 5756 (1993).

[45] G. W. Ford, M. Kac, and P. Mazur, J. Math. Phys. **6**, 504 (1965).

[46] B. J. Berne, J. P. Boon, and S. A. Rice, J. Chem. Phys. **45**, 1086 (1966); B. J. Berne and G. D. Harp, Adv. Chem. Phys. **17**, 63 (1970); G. D. Harp and B. J. Berne, Phys. Rev. A **2**, 975 (1970); J. M. Deutch and I. Oppenheim, J. Chem. Phys. **54**, 3547 (1971).

[47] G. R. Haynes and G. A. Voth, Phys. Rev. A **46**, 2143 (1992); J. B. Straus and G. A. Voth, J. Chem. Phys. **96**, 5460 (1992).

[48] G. van der Zwan and J. T. Hynes, J. Chem. Phys. **76**, 2993 (1982); J. T. Hynes, Discuss. Faraday Soc. **85**, 353 (1988).

[49] B. J. Gertner, J. P. Bergsma, K. R. Wilson, S. Lee, and J. T. Hynes, J. Chem. Phys. **86**, 1377 (1987).

[50] R. T. Grote and J. T. Hynes, J. Chem. Phys. **73**, 2715 (1980); *ibid.* **74**, 4465 (1981).

[51] G. van der Zwan and J. T. Hynes, J. Chem. Phys. **78**, 4174 (1983); G. van der Zwan and J. T. Hynes, Chem. Phys. **90**, 21 (1984); Y. I. Dakhnovskii and A. A. Ovchinnikov, Phys. Lett. **113A**, 147 (1985); E. Pollak, J. Chem. Phys. **85**, 865 (1986); S. C. Tucker, J. Phys. Chem. **97**, 1596 (1993).

[52] J. P. Bergsma, J. R. Reimers, K. R. Wilson, and J. T. Hynes, J. Chem. Phys. **85**, 5625 (1986); B. J. Gertner, K. R. Wilson, D. A. Zichi, S. Lee, and J. T. Hynes, Faraday Discuss. Chem. Soc. **85**, 297 (1988); B. J. Gertner, K. R. Wilson, and J. T. Hynes, J. Chem. Phys. **90**, 3537 (1989); G. Ciccotti, M. Ferrario, J. T. Hynes, and R. Kapral, *ibid.* **93**, 7137 (1990); W. P. Keirstead, K. R. Wilson, and J. T. Hynes, *ibid.* **95**, 5256 (1991); J. E. Straub, M. Borkovec, and B. J. Berne, *ibid.* **89**, 4833 (1988); R. Rey, E. Guàrdia, and J. A. Padró, *ibid.* **97**, 1343 (1992); R. M. Whitnell and K. R. Wilson, in *Review in Computational Chemistry*, Vol. 4, edited by K. B. Lipkowitz and D. B. Boyd (VCH, New York, 1993), p. 67; P. L. Geissler, C. Dellago, and D. Chandler, J. Phys. Chem. B **103**, 3706 (1999); D. G. Truhlar and B. C. Garrett, *ibid.* **104**, 1069 (2000).
[53] J. Horiuti, Bull. Chem. Soc. Jpn. **13**, 210 (1938); J. C. Keck, J. Chem. Phys. **32**, 1035 (1960).
[54] B. C. Garrett, D. G. Truhlar, R. S. Grev, and A. W. Magnuson, J. Phys. Chem. **84**, 1730 (1980).
[55] W. H. Miller, N. C. Handy, and J. E. Adams, J. Chem. Phys. **72**, 99 (1980).
[56] R. T. Skodje, D. G. Truhlar, and B. C. Garrett, J. Chem. Phys. **77**, 5955 (1982); R. T. Skodje, D. G. Truhlar, and B. C. Garrett, J. Phys. Chem. **85**, 3019 (1981).
[57] D.-h. Lu, T. N. Truong, V. S. Melissas, G. C. Lynch, Y.-P. Liu, B. C. Garrett, R. Steckler, A. D. Isaacson, S. N. Rai, G. C. Hancock, J. G. Lauderdale, T. Joseph, and D. G. Truhlar, Comput. Phys. Commun. **71**, 235 (1992).
[58] Y.-P. Liu, G. C. Lynch, T. N. Truong, D.-h. Lu, D. G. Truhlar, and B. C. Garrett, J. Am. Chem. Soc. **115**, 2408 (1993).
[59] S. Nosé, J. Chem. Phys. **81**, 511 (1984); S. Nosé, Mol. Phys. **52**, 255 (1984).
[60] M. P. Allen and D. J. Tildesley, *Computer Simulation of Liquids* (Oxford University Press, New York, 1987).
[61] M. Sceats, Adv. Chem. Phys. **70**, 357 (1988); E. A. Carter, G. Ciccotti, J. T. Hynes, and R. Kapral, Chem. Phys. Lett. **156**, 472 (1989).
[62] B. C. Garrett, M. J. Redmon, R. Steckler, D. G. Truhlar, K. K. Baldridge, D. Bartol, M. W. Schmidt, and M. S. Gordon, J. Phys. Chem. **92**, 1476 (1988).
[63] B. C. Garrett, T. Joseph, T. N. Truong, and D. G. Truhlar, Chem. Phys. **136**, 271 (1989).
[64] M. D. Hack, A. W. Jasper, Y. L. Volobuev, D. W. Schwenke, and D. G. Truhlar, J. Phys. Chem. A **103**, 6309 (1999).
[65] L. Melander and W. H. Saunders, Jr., *Reaction Rates of Isotopic Molecules* (Krieger, Malabar, FL, 1987).
[66] D. K. Bondi, J. N. L. Connor, B. C. Garrett, and D. G. Truhlar, J. Chem. Phys. **78**, 5981 (1983).
[67] B. C. Garrett, D. G. Truhlar, A. F. Wagner, and T. H. Dunning, Jr., J. Chem. Phys. **78**, 4400 (1983).
[68] W. H. Miller, J. Chem. Phys. **61**, 1823 (1974); B. C. Garrett and D. G. Truhlar, J. Phys. Chem. **83**, 1052 (1979).
[69] D. G. Truhlar and A. Kuppermann, J. Am. Chem. Soc. **93**, 1840 (1971).
[70] B. C. Garrett and D. G. Truhlar, J. Phys. Chem. **83**, 2921 (1979).